Universitat Ramon Llull

DOCTORAL THESIS

Title	**Drug delivery in photodynamic therapy: From pharmaceutics to animal testing**
Presented by	**María García Díaz**
Centre	**IQS School of engineering**
Department	**Organic Chemistry**
Directed by	**Prof. Santi Nonell Marrugat** **Prof. Margarita Mora Giménez**

C. Claravall, 1-3
08022 Barcelona
Tel. 936 022 200
Fax 936 022 249
E-mail: urlsc@sec.url.es
www.url.es

TABLE of CONTENTS

CHAPTER 3: TOWARDS the IDEAL PHOTOSENSITIZER

Characterization of new porphycenes

CHAPTER 4: LIPOSOMES AS VEHICLES FOR DELIVERY OF PHOTOSENSITIZING AGENTS

Developing the ideal formulation

Chapter 1
Introduction

Photosensitizers: From drug design to animal testing

The therapeutic properties of light have been known for thousands of years, but it was only in the last century that photodynamic therapy (PDT) was developed. As an emerging therapy for the treatment of a variety of diseases, there has been extensive research into the design of new photosensitizers and drug delivery systems. A general introduction to the drug discovery of a new photosensitizer and the aim of this thesis is given in this chapter.

1.1. PHOTODYNAMIC THERAPY OF CANCER: general aspects

Photodynamic therapy (PDT) involves the administration of a photoactive dye or photosensitizer (PS) that is able to produce reactive oxygen species (ROS) upon irradiation with light. When the PS absorbs a photon, an electron is promoted from the ground state to an electronically-excited state that can then undergo electron transfer (type I reaction) generating superoxide, hydrogen peroxide and hydroxyl radicals; or can transfer energy to molecular oxygen to produce highly cytotoxic singlet oxygen (type II reaction) (Fig. 1.1) [1]. Both mechanisms can produce the photo-oxidation of certain amino acids, pyrimidine and purine bases of DNA/RNA, and unsaturated lipids, leading to DNA damage and/or damage to the cytoplasmic membrane allowing leakage of cellular contents or inactivation of membrane transport systems [2].

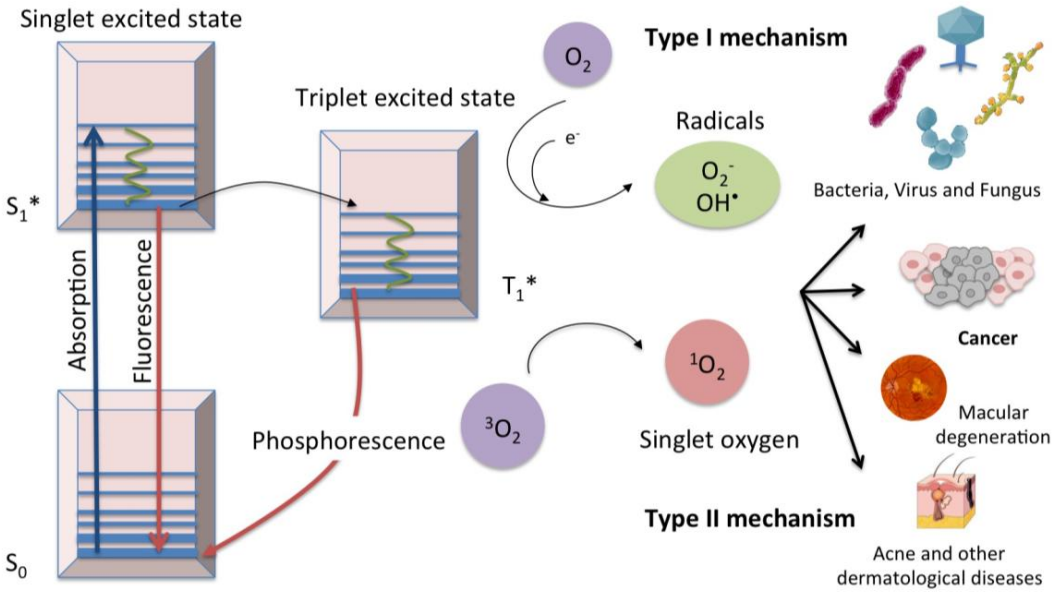

Figure 1.1. Jablosnki diagram depicting the possible photophysical properties and the mechanisms of ROS generation.

There are multiple applications of this therapy, including antimicrobial therapy, age-related macular degeneration (AMD), acne and dermatological diseases, and cancer.

Photodynamic therapy of cancer is particularly attractive because of its fundamental specificity and selectivity. As described above, PDT involves the combination of three individually non-toxic components (PS, visible light and molecular oxygen) to induce cellular and tissue effects. Thus, this treatment shows a dual selectivity that is produced by both a preferential uptake of the PS by the diseased tissue and the ability to confine activation of PS by restricting the illumination to that specific area.

Although it was initially considered that PDT-induced damage was confined to the treated site, it is now accepted that this therapy is endowed with multifactorial effects, which include direct tumor cell killing, damage to the tumor vasculature and activation of the immune system [1]. It is generally accepted that all three mechanisms are necessary for the optimal tumor damage. The relative contribution of these pathways depends upon the PS used, the tissue being treated, and the treatment conditions.

ROS generated by PDT can kill cells directly by apoptosis, necrosis and/or autophagy if the PS has been taken up by tumor cells. However, complete tumor eradication is not always fully realized by this mechanism mainly due to the non-homogeneous distribution of the PS and oxygen concentration within the tumor [1,3].

PDT also damages the tumor-associated vasculature. An initial blanching and vasoconstriction of the tumor vessels is followed by acute blood stasis, hemorrhage and the formation of platelet aggregates, that provokes the vascular shut-down. As a result, tumor cells become deprived from oxygen and nutrient supply, leading to the elimination of the tumor [4,5].

PDT triggers several cell-signaling cascades and the release of cell fragments, cytokines and inflammatory mediators that stimulate a complex interplay between the innate and the adaptive arms of the immune system to recognize and destroy tumor cells even at isolated locations [6-8].

1.2. DRUG DISCOVERY

In the fields of medicine, biotechnology and pharmacology, drug discovery is the process by which drugs are discovered or designed. The process of drug discovery for PDT involves the identification and synthesis of the PS, its photophysical characterization, the development of a formulation and assays for therapeutic PDT efficacy both *in vitro* and *in vivo.* Once a compound has shown its value in these tests, it will begin the process of drug development prior to clinical trials.

1.2.1. Photosensitizers

Photosensitizers (PSs) are exogenous or endogenous chemicals that cause sensitization to light. Exogenous PSs tend to be relatively large molecules and are usually administered parentally, while the endogenous PS protoporphyrin IX (PpIX) can be induced by topical delivery of 5-aminolevulinic acid (ALA) [9].

An ideal PS agent should be single pure compound with easy and low cost synthesis, and should have chemical and physical stability. It should have a high absorption peak between 600 and 800 nm, the so-called therapeutic window, which allows the maximum light penetration through the tissue with the minimum light scattering. It should have high singlet oxygen quantum yield for high photodynamic efficiency but also be fluorescent and photostable to facilitate monitoring. It should be devoid of any toxicity without light, and also show selective uptake, rapid clearance from normal tissues to minimize skin photosensitivity and other side effects, and microlocalization to sensitive cellular/subcellular targets (e.g. mitochondria) [10,11].

Since the development of porfimer sodium (Photofrin®) in the last part of the 20th Century, there has been a concerted effort to develop new, more potent, tumor-specific agents with the overall aim of improving therapeutic outcomes for patients. Although Photofrin® is still the most widely used PS, the product has some disadvantages, including long-lasting skin photosensitivity and relatively low absorbance at 630 nm. After Photofrin® several hundred compounds, referred to as second-generation PSs, have been proposed as potentially useful for anticancer PDT. The main classes are synthetic porphyrin, porphycenes, chlorins, bacteriochlorins and phthalocyanines. Their core structures are depicted in Fig. 1.2. Table 1.1 displays the most promising PSs that have been used clinically for cancer PDT (whether approved or in trials).

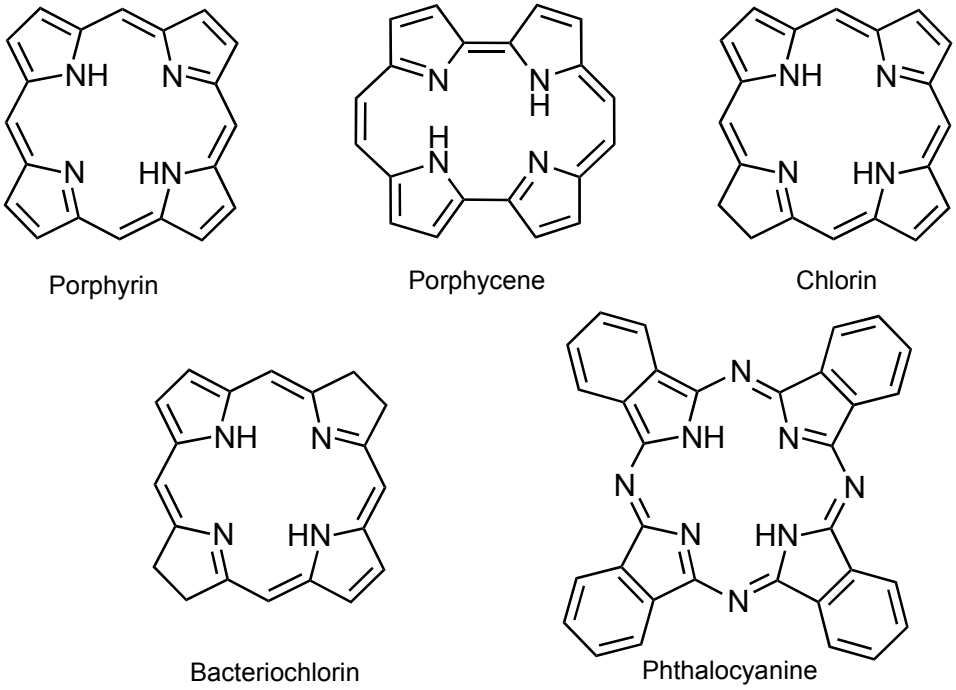

Figure 1.2. Core structures of the main kinds of second-generation PSs.

Table 1.1. Clinically applied photosensitizers. From [11]

PHOTOSENSITIZER	STRUCTURE	WAVELENGTH, nm	APPROVED	TRIALS	CANCER TYPES
Porfimer sodium (Photofrin) (HPD)	Porphyrin	630	Worldwide		Lung, esophagus, bile duct, bladder, brain, ovarian
ALA	Porphyrin precursor	635	Worldwide		Skin, bladder, brain, esophagus
ALA esters	Porphyrin precursor	635	Europe		Skin, bladder
Temoporfin (Foscan) (mTHPC)	Chlorine	652	Europe	United States	Head and neck, lung, brain, skin, bile duct
Verteporfin	Chlorine	690	Worldwide (AMD)	United Kingdom	Ophthalmic, pancreatic, skin
HPPH	Chlorin	665		United States	Head and neck, esophagus, lung
SnEt2 (Purlytin)	Chlorin	660		United States	Skin, breast
Talaporfin (LS11, MACE, NPe6)	Chlorin	660		United States	Liver, colon, brain
Ce6-PVP (Fotolon), Ce6 derivatives (Radachlorin, Photodithazine)	Chlorin	660		Belarus, Russia	Nasopharyngeal, sarcoma, brain
Silicon phthalocyanine (Pc4)	Phthalocyanine	675		United States	Cutaneous T-cell lymphoma
Padoporfin (TOOKAD)	Bacteriochlorin	762		United States	Prostate
Motexafin lutetium (Lutex)	Texaphyrin	732		United States	Breast

Our group has focused the interest in the porphycene family. Porphycenes are structural isomers of porphyrins that have many unique properties and features [12]. The most relevant feature of the porphycene ring is its lower structural symmetry that results in 20-fold larger absorption coefficients in the red part of the spectrum compared to porphyrins. Since the synthesis of the first porphycene in 1986 [13], a variety of substituted derivatives have been prepared [14]. The excellent porphycene's photophysical properties, as well as its ability to photoinactivate several cell lines [15-18], promote the porphycenes as promising PSs for PDT treatments.

1.2.2. Drug delivery systems

Most PS molecules tend to be highly hydrophobic and therefore aggregate easily in aqueous environment [19]. The presence of hydrophobic interactions lowers the efficiency of the PS, which must be in monomeric form to be photoactive. Moreover, selective accumulation of the PS in diseases tissues is required to minimize unwanted side-effects result from damage to healthy cells. Thus, considerable efforts have been directed at designing delivery systems that can incorporate PS in monomeric form without diminishing its activity, and without causing any harmful effects *in vivo* [20]. Different strategies have been investigated. Fig. 1.3 shows a selected representation of the drug delivery systems most used for PDT.

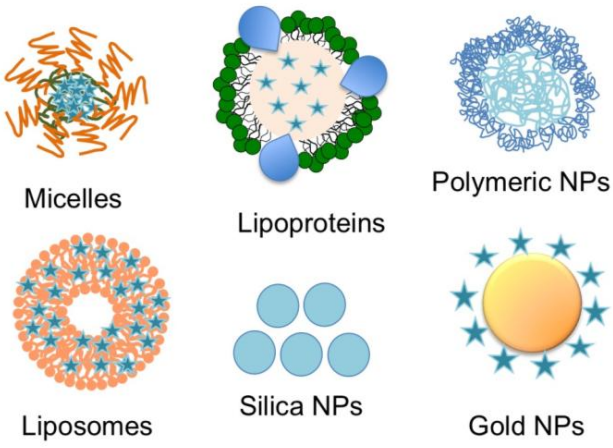

Figure 1.3. Drug delivery systems most used in PDT.

Polymeric nanoparticles (NPs) have recently emerged as a promising tool for the delivery of drugs in PDT, mainly because their flexibility toward surface modification and the possibility of being loaded with multiple components such as targeting ligands and contrast agents. A variety of polymeric NPs has been developed including synthetic polymers like polylactide-polyglycolide copolymers (PLGA), N-(2-hydroxypropyel)methacrylamide (HPMA), and polyacrylamide (PAA). Natural polymers composed of polysaccharides, such as chitosan and alginate, and proteins such as albumin, and collagen, have also been used [21-24].

Otherwise, silica NPs have several advantages as carriers for PDT agents: their particle size, shape, porosity and mono-dispersibility can be easily controlled during their preparation. They are pH stable and are not subject to microbial attack. Furthermore, a variety of precursors and methods are available for their synthesis allowing numerous PDT drugs to be encapsulated. Although these NPs do not release the entrapped PS, the porosity of the silica wall permeates the produced singlet oxygen and the desired phototoxic effect is maintained even in the encapsulated form [23,25].

Gold NPs have been used in two ways in PDT: firstly as drug-delivery platforms in a similar manner to other inorganic NPs [26]; secondly as surface plasmon-enhanced agents taking account of the non-linear-optical fields associated with very close distances to metal NPs [27,28].

Lipoproteins are naturally occurring NPs composed of a mixture of specific proteins, phospholipids and cholesterol with a hydrophobic core. The family consists of chylomicrons, very low density lipoproteins (VLDL), low density lipoproteins (LDL) and high density lipoproteins (HDL). Their small size (less than 30 nm) allows them to penetrate deeply into tumors. Furthermore, LDL has innate cancer targeting potential as LDL receptors are overexpressed on malignant cells [29].

Alternatively, micelles are suitable for the formulation of PSs. Their hydrophobic core can accommodate hydrophobic drugs, whereas their hydrophilic shell, which is usually composed of PEG, in combination with their small size (10-100 nm) results in long circulation times and selective accumulation at the tumor site. Several components have been studied for loading PS. Pluronic micelles, polymeric micelles using poly(ethylene glycol)-b-poly(caprolactone) (PEG-PCL) or poly(ethylene glycol)-b-poly(DL-lactic acid) (PEG-PLA) diblock copolymers, lipid-based PEG-PE or Cremophor EL have been extensively used for loading PSs for PDT [30,31].

Liposomes have far been the most intensively studied carrier system for PS, therapeutic drugs and cosmetic delivery due to their unique properties [32-36]. Conventional liposomes are highly biocompatible and biodegradable nanocarriers composed of a unilamellar or multilamellar phospholipid bilayer surrounding an aqueous inner core. In fact, they can contain a wide variety of hydrophilic and hydrophobic diagnostic or therapeutic agents, providing a larger drug payload per particle and protecting encapsulated agents from metabolic processes [37].

Among all the options, our group has opted for liposomes for the delivery of photosensitizing agents [38-40]. Once the PS has been incorporated in the liposomes, it can be delivered to cells in two interlocking ways, modulated by the nature of lipids and type of cell: cationic liposomes tend to fuse with cell membranes or endosomes and release its contents into the cytosol, whereas neutral or negatively-charged liposomes can be taken up by endocytosis and then disintegrated in endosomes or lysosomes, again releasing the active drug into the cell [41,42].

Due to the fast angiogenesis in malignant tissue, tumor vessel walls show an enhanced vascular permeability allowing liposomes to passively accumulate in tumor tissue at high concentrations [33]. However, such “conventional” liposomes have the drawback of a short plasma half-life *in vivo*, of the order of minutes. This is firstly due to rapid lipid exchange between the liposomes and lipoproteins and the easy opsonization by plasma proteins. To improve the pharmacokinetics and antitumor therapeutic efficacy, sterically stabilized liposomes were developed [43]. The surface of the liposome is decorated with hydrophilic carbohydrates or polymers, such as monosialoganglioside or polyethylene glycol, in order to extend the *in vivo* liposome circulating time.

Various strategies have been investigated to trigger the release of the encapsulated drug from liposomes at the optimal location and time, such as pH-triggered and redox-triggered release [44]. Some methods have been applied for he release of PS specifically at tumor tissue by stimuli such as light, heat or ultrasound [45].

Targeted drug delivery systems

Ideally, PDT holds the promise of dual selectivity due to a preferential tumor uptake of the PS and the restricted illuminated area for an improved selectivity. However, confined irradiation is not possible, leading to some phototoxicity to surrounding normal tissues. Moreover, several cases of prolonged skin photosensitivity have been reported

[46]. Targeted drug delivery systems are one of the strategies proposed to solve these problems underlying non-specific PS accumulation. Active targeting encompasses the strategy of coupling a specific entity to the surface of the NP, enhancing their selective interaction with target cells recognized by specific markers. While monoclonal antibodies have received the most attention [47,48], biochemical, metabolic and physiological alterations of tumor cells offer numerous other potent targets to exploit during the delivery of PS. Folic acid (vitamin B9) is essential for the proliferation and maintenance of cells. The overexpression of folate receptor on a variety of epithelial cancer cells and the high affinity of folate for its receptor has attracted wide attention as a targeting agent for tumor selectivity [49,50]. Small peptides that selectively recognize tumor cells represent another excellent approach for targeting therapies [51], and hyaluronic acid recognizes CD44, known as the hyaluronic acid receptor, which is involved in cell adhesion and is also overexpressed on many cancer cells [52,53].

1.2.3. *In vitro* tests

PDT efficiency is generally tested *in vitro* as a first approximation to the photodynamic action of a PS. Although PDT can induce many cellular and molecular signaling pathways events in cells, its main purpose is to induce cell death. The concentration, physicochemical properties and subcellular localization of the PS, the concentration of oxygen, the appropriate wavelength and intensity of light, as well as the cell type specific properties may all influence the mode and the extent of cell death [54].

Modes of cell death

Cells can undergo three different types of cell death after PDT. Necrosis, referred to as accidental cell death, is considered to be an unprogrammed process. It is a violent and quick form of degeneration characterized by *in vitro* cytoplasm swelling, devastation of organelles and disruption of the plasma membrane, leading to the release of intracellular contents and *in vivo* inflammation [55].

A different type of cell death termed apoptosis represents regulated cell suicide. Apoptosis requires transcriptional activation of specific genes, including the activation of endonucleases, consequent DNA degradation, and activation of caspases. The organelles and plasma membrane tend to retain their structure for quite a long period. *In vitro,* apoptotic cells are usually fragmented into multiple membrane enclosed

spherical vesicles. *In vivo,* these apoptotic bodies are scavenged by phagocytes, inflammation is prevented, and cells die in an immunologically controlled way [56,57]. In spite of this fact, researchers have recently discovered a new apoptotic cell death modality called –"immunogenic apoptosis", which is provoked by the endoplasmic reticulum (ER) stress accompanied by ROS and is able to trigger an effective dendritic cell-based antitumor immune response [58].

Autophagy is a process whereby a portion of the cytosol, usually containing cellular organelles, is sequestered by a double membrane. The resulted vesicle then fuses with a lysosome, the contents are digested, and can be recycle during periods of starvation. There is also evidence that autophagy can be a cell-death mode under appropriate circumstances, accompanying apoptosis after ER photodamage [59].

3D cell cultures

Tissues and organs are three-dimensional (3D). However, the ability to understand their formation, function and pathology has often depended on two-dimensional (2D) cell culture studies. Standard cell cultures can differ considerable in their morphology, cell-cell and cell-matrix interactions, and differentiation from those growing in more physiological 3D environments. *In vitro* 3D tissue models provide an approach that bridges the gap between traditional cell culture and animal models [60]. 3D-cell scaffolds have been developed within the tissue engineering field for tissue regeneration and organ replacement [61,62]. However, researchers in the photodynamic field have also followed this strategy in order to better mimic the cancer tissue environment and optimize the parameters for an efficient PDT outcome *in vivo*. Spheroids have so far been the most intensively studied 3D system for PDT and a wide variety of therapy studying the effects on fundamental mechanisms, including regulation of proliferation, cell death, differentiation and metabolism. Multicellular spheroids are formed by culturing cells in spinner flasks or agar-coated culture plates. Under these conditions, cells form spherical clusters that can survive for weeks and can reach sizes of up to several millimeters in diameter. Multicellular spheroids offer a simple and highly reproducible model that contains many of the features of natural tissue [63]. It has been found that oxygen gradients characteristics of spheroids produce heterogeneous response to PDT [64]. They are also well suited for investigating the utility of therapies on tumor cell invasion [65]. The study of PDT-induced vascular damage has been recently investigated using a sophisticated spheroid-chick chorioallantoic membrane (CAM) system [66].

A basement membrane cell culture approach has been used for the *in vitro* model of an ovarian metastatic cancer [67]. This strategy uses a synthetic media that contains collagen and growth factors that mimic the extracellular matrix (ECM).

In a similar approach, a novel hydrogel-based 3D culture model has been developed for better predict the PDT outcome (see chapter 7). The model uses a self-assembling RAD16-I scaffold that forms a network of interweaving nanofibers of 10-20 nm diameter and 50-200 nm pore size, surrounding cells in a similar manner to the natural extracellular matrix and, thereby, mimicking the *in vivo* cellular environment.

Ex-vivo skin models have been used for addressing the photodynamic potential of some PS for skin cancer and other malignancies [68,69].

1.2.4. *In vivo* tests

The final step of the PS efficacy evaluation before jump to clinical trials is the *in vivo* (animal) testing. The animals most used for PDT purposes are small rodents such as mice and rats, although rabbits, pigs, dogs and cats have also been used. The standard protocol involves the subcutaneous inoculation of cancer cells into the desired zone, a waiting time until the development of the tumor and the evaluation of tumor growth, survival and other effects (e.g. immune response activation) after PDT treatment. Even zebra fish have been used as model for studying synergistic effects between PDT and a novel ultrasound activated therapy [70]. The chick chorioallantoic membrane (CAM) model is useful for the assessment of PDT-induced vascular damage [71,72]. This *in vivo* model has the advantage of providing an easily accessible neovascular net in a transparent matrix, and therefore vascular effects and drug pharmacokinetics are easily measured.

1.3. OBJECTIVES

The main goal of this thesis is to study the efficacy of new porphycene photosensitizers and the influence of drug delivery systems in photodynamic therapy. This is divided into the following specific objectives:

- Characterization of the photophysical properties of new porphycene-based photosensitizers.
- Development of liposomal formulations for the encapsulation of photosensitizing agents and investigation of the potential of targeting strategy.
- Assessment of the antitumor potential of a new porphycene photosensitizer *in vitro* and *in vivo*.
- Assessment of the potential of new models for predicting the photodynamic therapy outcome *in vitro.*

1.4. REFERENCES

[1] T.J. Dougherty, C.J. Gomer, B.W. Henderson, G. Jori, D. Kessel, M. Korbelik, et al. Photodynamic therapy, J. Natl. Cancer Inst. 90 (1998) 889-905.

[2] A.P. Castano, T.N. Demidova, M.R. Hamblin. Mechanisms in photodynamic therapy: part two: cellular signaling, cell metabolism and modes of cell death, Photodiagnosis Photodyn. Ther. 2 (2005) 1-23.

[3] D.E.J.G. Dolmans, D. Fukumura, R.K. Jain. Photodynamic therapy for cancer, Nat. Rev. Cancer. 3 (2003) 380-387.

[4] B. Chen, B.W. Pogue, J.M. Luna, R.L. Hardman, P.J. Hoopes, T. Hasan. Tumor vascular permeabilization by vascular-targeting photosensitization: effects, mechanism, and therapeutic implications, Clin. Cancer Res. 12 (2006) 917-923.

[5] B. Krammer. Vascular effects of photodynamic therapy, Anticancer Res. 21 (2001) 4271-4277.

[6] P. Mroz, J.T. Hashmi, Y.Y. Huang, N. Lange, M.R. Hamblin. Stimulation of anti-tumor immunity by photodynamic therapy, Expert Rev. Clin. Immunol. 7 (2011) 75-91.

[7] A.P. Castano, P. Mroz, M.R. Hamblin. Photodynamic therapy and anti-tumour immunity, Nat. Rev. Cancer. 6 (2006) 535-545.

[8] S.O. Gollnick, B. Owczarczak, P. Maier. Photodynamic therapy and anti-tumor immunity, Lasers Surg. Med. 38 (2006) 509-515.

[9] M.J. Garland, C.M. Cassidy, D. Woolfson, R.F. Donnelly. Designing photosensitizers for photodynamic therapy: strategies, challenges and promising developments, Future Med. Chem. 1 (2009) 667-691.

[10] B.C. Wilson, M.S. Patterson. The physics, biophysics and technology of photodynamic therapy, Phys .Med. Biol. 53 (2008) 61-109.

[11] P. Agostinis, K. Berg, K.A. Cengel, T.H. Foster, A.W. Girotti, S.O. Gollnick, et al. Photodynamic therapy of cancer: An update, CA Cancer. J. Clin. 61 (2011) 250-281.

[12] J.C. Stockert, M. Cañete, A. Juarranz, A. Villanueva, R.W. Horobin, J.I. Borrell, et al. Porphycenes: facts and prospects in photodynamic therapy of cancer, Curr. Med. Chem. 14 (2007) 997-1026.

[13] E. Vogel, M. Kocher, H. Schmickler, J. Lex. Porphycene - a Novel Porphin Isomer, Angew. Chem.-Int. Edit. Engl. 25 (1986) 257-259.

[14] C. Richert, J.M. Wessels, M. Muller, M. Kisters, T. Benninghaus, A.E. Goetz. Photodynamic antitumor agents: beta-methoxyethyl groups give access to functionalized porphycenes and enhance cellular uptake and activity, J. Med. Chem. 37 (1994) 2797-2807.

[15] M. Guardiano, R. Biolo, G. Jori, K. Schaffner. Tetra-n-propylporphycene as a tumour localizer: pharmacokinetic and phototherapeutic studies in mice, Cancer Lett. 44 (1989) 1-6.

[16] M. Cañete, M. Lapena, A. Juarranz, V. Vendrell, J.I. Borrell, J. Teixido, et al. Uptake of tetraphenylporphycene and its photoeffects on actin and cytokeratin elements of HeLa cells, Anticancer Drug Des. 12 (1997) 543-554.

[17] A. Villanueva, M. Cañete, S. Nonell, J.I. Borrell, J. Teixido, A. Juarranz. Photodamaging effects of tetraphenylporphycene in a human carcinoma cell line, Anticancer Drug Des. 11 (1996) 89-99.

[18] M. García-Díaz, D. Sánchez-García, J. Soriano, M.L. Sagristà, M. Mora, Á Villanueva, et al. Temocene: the porphycene analogue of temoporfin (Foscan®), Med. Chem. Commun. 2 (2011) 616-619.

[19] J.P. Keene, D. Kessel, E.J. Land, R.W. Redmond, T.G. Truscott. Direct Detection of Singlet Oxygen Sensitized by Hematoporphyrin and Related-Compounds, Photochem. Photobiol. 43 (1986) 117-120.

[20] V.P. Torchilin, Nanoparticulates As Drug Carriers, Imperial College Press 2006.

[21] J. Panyam, V. Labhasetwar. Biodegradable nanoparticles for drug and gene delivery to cells

and tissue, Adv. Drug Deliv. Rev. 55 (2003) 329-347.

[22] Y.E. Lee, R. Kopelman. Polymeric nanoparticles for photodynamic therapy, Methods Mol. Biol. 726 (2011) 151-178.

[23] D.K. Chatterjee, L.S. Fong, Y. Zhang. Nanoparticles in photodynamic therapy: an emerging paradigm, Adv. Drug Deliv. Rev. 60 (2008) 1627-1637.

[24] D. Bechet, P. Couleaud, C. Frochot, M.L. Viriot, F. Guillemin, M. Barberi-Heyob. Nanoparticles as vehicles for delivery of photodynamic therapy agents, Trends Biotechnol. 26 (2008) 612-621.

[25] P. Couleaud, V. Morosini, C. Frochot, S. Richeter, L. Raehm, J.O. Durand. Silica-based nanoparticles for photodynamic therapy applications, Nanoscale. 2 (2010) 1083-1095.

[26] Y. Cheng, A. C Samia, J.D. Meyers, I. Panagopoulos, B. Fei, C. Burda. Highly efficient drug delivery with gold nanoparticle vectors for in vivo photodynamic therapy of cancer, J. Am. Chem. Soc. 130 (2008) 10643-10647.

[27] B. Khlebtsov, E. Panfilova, V. Khanadeev, O. Bibikova, G. Terentyuk, A. Ivanov, et al. Nanocomposites containing silica-coated gold-silver nanocages and Yb-2,4-dimethoxyhematoporphyrin: multifunctional capability of IR-luminescence detection, photosensitization, and photothermolysis, ACS Nano 5 (2011) 7077-7089.

[28] A.M. Fales, H. Yuan, T. Vo-Dinh. Silica-coated gold nanostars for combined surface-enhanced Raman scattering (SERS) detection and singlet-oxygen generation: a potential nanoplatform for theranostics, Langmuir 27 (2011) 12186-12190.

[29] K.K. Ng, J.F. Lovell, G. Zheng. Lipoprotein-inspired nanoparticles for cancer theranostics, Acc. Chem. Res. 44 (2011) 1105-1113.

[30] Y. Konan, R. Gurny, E. Allémann. State of the art in the delivery of photosensitizers for photodynamic therapy, J. Photochem. Photobiol. B:Biol. 66 (2002) 89-106.

[31] C.F. van Nostrum. Polymeric micelles to deliver photosensitizers for photodynamic therapy, Adv. Drug Deliv. Rev. 56 (2004) 9-16.

[32] C.S. Jin, G. Zheng. Liposomal nanostructures for photosensitizer delivery, Lasers Surg. Med. 43 (2011) 734-748.

[33] A.S. Derycke, P.A.d. Witte. Liposomes for photodynamic therapy, Adv. Drug Deliv. Rev. 56 (2004) 17-30.

[34] R.R. Sawant, V.P. Torchilin. Liposomes as 'smart' pharmaceutical nanocarriers, Soft Matter. 6 (2010) 4026-4044.

[35] R.A. Schwendener. Liposomes in biology and medicine, Adv. Exp. Med. Biol. 620 (2007) 117-128.

[36] D.D. Lasic, Y. Barenholz, Handbook of nonmedical application of liposomes: vol. I - IV, CRC Press Inc 1996.

[37] D. Di Paolo, F. Pastorino, C. Brignole, D. Marimpietri, M. Loi, M. Ponzoni, et al. Drug delivery systems: application of liposomal anti-tumor agents to neuroectodermal cancer treatment, Tumori. 94 (2008) 246-253.

[38] F. Postigo, M.L. Sagrista, M.A. De Madariaga, S. Nonell, M. Mora. Photosensitization of skin fibroblasts and HeLa cells by three chlorin derivatives: Role of chemical structure and delivery vehicle, Biochim. Biophys. Acta. 1758 (2006) 583-596.

[39] F. Postigo, M. Mora, M.A. De Madariaga, S. Nonell, M.L. Sagrista. Incorporation of hydrophobic porphyrins into liposomes: characterization and structural requirements, Int. J. Pharm. 278 (2004) 239-254.

[40] M.L. Sagrista, F. Postigo, M.A.D. Madariaga, R.M. Pinto, S. Caballero, A. Bosch, et al. Photodynamic inactivation of viruses by immobilized chlorin-containing liposomes, J. Porphyrins Phthalocyanines 13 (2009) 578-588.

[41] A. Sharma, U.S. Sharma. Liposomes in drug delivery: Progress and limitations, Int. J. Pharm. 154 (1997) 123.

[42] Duzgune&scedil, N. , S. Nir. Mechanisms and kinetics of liposome-cell interactions, Adv. Drug Deliv. Rev. 40 (1999) 3-18.

[43] D.D. Lasic, F.J. Martin, A. Gabizon, S.K. Huang, D. Papahadjopoulos. Sterically stabilized liposomes: a hypothesis on the molecular origin

of the extended circulation times, Biochim. Biophys. Acta. 1070 (1991) 187-192.

[44] X. Guo, F.C. Szoka Jr. Chemical approaches to triggerable lipid vesicles for drug and gene delivery, Acc. Chem. Res. 36 (2003) 335-341.

[45] V. Torchilin. Multifunctional and stimuli-sensitive pharmaceutical nanocarriers, Eur. J. Pharm. Biopharm. 71 (2009) 431-444.

[46] S.B. Brown, E.A. Brown, I. Walker. The present and future role of photodynamic therapy in cancer treatment, Lancet Oncol. 5 (2004) 497-508.

[47] N. Kameyama, S. Matsuda, O. Itano, A. Ito, T. Konno, T. Arai, et al. Photodynamic therapy using an anti-EGF receptor antibody complexed with verteporfin nanoparticles: a proof of concept study, Cancer Biother. Radiopharm. 26 (2011) 697-704.

[48] A.J. Bullous, C.M. Alonso, R.W. Boyle. Photosensitiser-antibody conjugates for photodynamic therapy, Photochem. Photobiol. Sci. 10 (2011) 721-750.

[49] N. Parker, M.J. Turk, E. Westrick, J.D. Lewis, P.S. Low, C.P. Leamon. Folate receptor expression in carcinomas and normal tissues determined by a quantitative radioligand binding assay, Anal. Biochem. 338 (2005) 284-293.

[50] M. Garcia-Diaz, S. Nonell, A. Villanueva, J.C. Stockert, M. Canete, A. Casado, et al. Do folate-receptor targeted liposomal photosensitizers enhance photodynamic therapy selectivity? Biochim. Biophys. Acta. 1808 (2011) 1063-1071.

[51] H.J. Hah, G. Kim, Y.E. Lee, D.A. Orringer, O. Sagher, M.A. Philbert, et al. Methylene blue-conjugated hydrogel nanoparticles and tumor-cell targeted photodynamic therapy, Macromol. Biosci. 11 (2011) 90-99.

[52] V.M. Platt, F.C. Szoka Jr. Anticancer therapeutics: targeting macromolecules and nanocarriers to hyaluronan or CD44, a hyaluronan receptor, Mol. Pharm. 5 (2008) 474-486.

[53] F. Li, B.C. Bae, K. Na. Acetylated Hyaluronic Acid/Photosensitizer Conjugate for the Preparation of Nanogels with Controllable Phototoxicity: Synthesis, Characterization, Autophotoquenching Properties, and in vitro Phototoxicity against HeLa Cells, Bioconjug. Chem. 21 (2010) 1312-1320.

[54] C.A. Robertson, D.H. Evans, H. Abrahamse. Photodynamic therapy (PDT): a short review on cellular mechanisms and cancer research applications for PDT, J. Photochem. Photobiol. B: Biol. 96 (2009) 1-8.

[55] C.N. Zhou. New trends in photobiology - Mechanisms of tumor necrosis induced by photodynamic therapy, J. Photochem. Photobiol. B:Biol. 3 (1989) 299-318.

[56] N.L. Oleinick, R.L. Morris, I. Belichenko. The role of apoptosis in response to photodynamic therapy: what, where, why, and how, Photochem. Photobiol. Sci. 1 (2002) 1-21.

[57] K. Plaetzer, T. Kiesslich, C.B. Oberdanner, B. Krammer. Apoptosis following photodynamic tumor therapy: Induction, mechanisms and detection, Curr. Pharm. Des. 11 (2005) 1151-1165.

[58] A.D. Garg, D. Nowis, J. Golab, P. Vandenabeele, D.V. Krysko, P. Agostinis. Immunogenic cell death, DAMPs and anticancer therapeutics: an emerging amalgamation, Biochim. Biophys. Acta. 1805 (2010) 53-71.

[59] D. Kessel. Death pathways associated with photodynamic therapy, Med. Laser Appl. 21 (2006) 219-224.

[60] K.M. Yamada, E. Cukierman. Modeling tissue morphogenesis and cancer in 3D, Cell. 130 (2007) 601-610.

[61] L.G. Griffith, G. Naughton. Tissue engineering--current challenges and expanding opportunities, Science. 295 (2002) 1009-1014.

[62] L.G. Griffith, M.A. Swartz. Capturing complex 3D tissue physiology in vitro, Nat. REv. Mol. Cell Biol. 7 (2006) 211-224.

[63] T.T. Goodman, C.P. Ng, S.H. Pun. 3-D tissue culture systems for the evaluation and optimization of nanoparticle-based drug carriers, Bioconjug. Chem. 19 (2008) 1951-1959.

[64] S.J. Madsen, C.H. Sun, B.J. Tromberg, V. Cristini, N. De Magalhaes, H. Hirschberg.

Multicell tumor spheroids in photodynamic therapy, Lasers Surg. Med. 38 (2006) 555-564.

[65] H. Hirschberg, C. Sun, S. Madsen. Reduction of the invasiveness of human glioma cells by ALA-mediated photodynamic therapy, Proc. SPIE. 6078 (2006) 60782X.

[66] N. De Magalhaes, L.L. Liaw, L. Li, A. Liogys, S.J. Madsen, H. Hirschberg, et al. Investigating the effects of combined photodynamic and anti-angiogenic therapies using a three-dimensional in-vivo brain tumor system, Proc. SPIE. 6078 (2006) 607830.

[67] I. Rizvi, J.P. Celli, C.L. Evans, A.O. Abu-Yousif, A. Muzikansky, B.W. Pogue, et al. Synergistic enhancement of carboplatin efficacy with photodynamic therapy in a three-dimensional model for micrometastatic ovarian cancer, Cancer Res. 70 (2010) 9319-9328.

[68] E. Gemenetzidis, O. Shavorskaya, Y.Z. Xu, G. Trigiante. Topical 4-thiothymidine is a viable photosensitiser for the photodynamic therapy of skin malignancies, J. Dermatolog Treat. (2011).

[69] P. Babilas, E. Kohl, T. Maisch, H. Backer, B. Gross, A.L. Branzan, et al. In vitro and in vivo comparison of two different light sources for topical photodynamic therapy, Br. J. Dermatol. 154 (2006) 712-718.

[70] T.J. Lewis. Toxicity and cytopathogenic properties toward human melanoma cells of activated cancer therapeutics in zebra fish, Integr. Cancer. Ther. 9 (2010) 84-92.

[71] B. Pegaz, E. Debefve, J.P. Ballini, G. Wagnieres, S. Spaniol, V. Albrecht, et al. Photothrombic activity of m-THPC-loaded liposomal formulations: pre-clinical assessment on chick chorioallantoic membrane model, Eur. J. Pharm. Sci. 28 (2006) 134-140.

[72] N. Lange, J.P. Ballini, G. Wagnieres, H. van den Bergh. A new drug-screening procedure for photosensitizing agents used in photodynamic therapy for CNV, Invest. Ophthalmol. Vis. Sci. 42 (2001) 38-46.

Chapter 2

General techniques and methods

Photobiology: the science of light and life

Photobiology deals with the interaction of light with living organisms, from cellular to *in vivo* live specimens. This chapter describes the general techniques and methods involving both light and life: specific methods and techniques used for the determination of photophysical properties in the light-induced reaction processes; and the basics of liposome preparation and characterization, cell culture protocols and animal handling. Specific details will be described in the experimental section of each chapter.

2.1. STEADY-STATE OPTICAL TECHNIQUES

2.1.1. Absorbance and transmittance

Spectra were recorded in both a Varian Cary 4E spectrophotometer (Varian, Palo Alto, CA) and a Cary 6000i UV-Vis-NIR spectrophotometer (Agilent Technologies, Santa Clara, CA). For diffuse transmittance measurements of cell suspensions, the spectrophotometer was equipped with 110 mm-diameter integrating sphere and a high performance photomultiplier tube. Integrating spheres have the ability to collect most reflected or transmitted radiation from turbid, translucent or opaque samples, removing any directional preferences and presenting an integrated signal to the detector.

2.1.2. Emission

Fluorescence emission and excitation spectra were recorded in both a Spex Fluoromax-2 spectrofluorometer and a Fluoromax-4 spectrofluorometer (Horiba Jobin-Ybon, Edison, NJ). The absorbance of the sample was ensured to be less than 0.05 in the overlap region between absorption and emission to avoid inner filter effects in the measurement of fluorescence.

Method

Fluorescence quantum yield (Φ_F)

The fluorescence quantum yields were determined from the comparison of the area under the corrected emission curves of optically-matched solutions of the sample to that of a suitable reference (*i.e.* with a similar emission spectrum as the sample). The quantum yields (Φ_F) were determined by means of Eq. 2.1:

$$\Phi_F(\text{sample}) = \frac{F_{sample} \cdot n_{sample}^2}{F_{ref} \cdot n_{ref}^2} \cdot \Phi_F(\text{ref}) \qquad (2.1)$$

where F_i is the fluorescence intensity integrated over the entire emission spectrum corrected by the absorption factor ($1\text{-}10^{-A}$) and n_i is the refractive index of the solvent used in each case.

2.2. TIME-RESOLVED OPTICAL TECHNIQUES

The time-resolved techniques used in this work involve the observation, through absorption or emission, of excited states or other reaction intermediates generated upon pulsed-laser irradiation of a sample. The formation of a large concentration of transient species upon absorption of light produced a change in the intensity of an analyzing beam (in the case of absorption spectroscopy) or in the intensity that emerges from the sample (in the case of emission spectroscopy), which the system is able to monitor with time resolution.

2.2.1. Time-correlated single photon counting (TCSPC)

Time-correlated Single Photon Counting is the most commonly used technique for singlet state lifetime determination. It is based on the detection of single photons of a periodical light signal, the measurement of the detection times of the individual photons and the reconstruction of the waveform form the individual time measurements. TCSPC technique makes use of the fact for low-level, high-repetition-rate pulses, the produced light intensity is so low that the probability of detecting one photon in one signal period is much less than one. Therefore, it is not necessary to provide for the possibility of detecting several photons in one signal period. It is sufficient to record the photons, measure their time in the signal period, and build up a histogram of the photon times.

The principle is shown in Fig. 2.1:

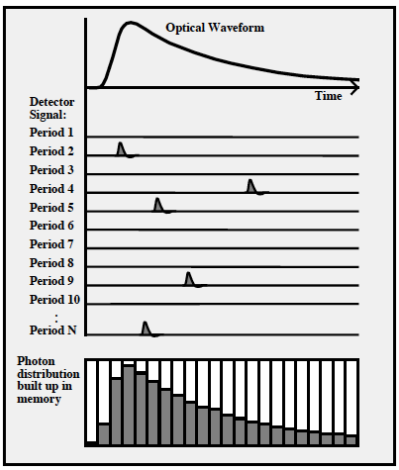

Figure 2.1. Principle of classic time-correlated single photon counting. From [1]

In most cases, the lifetime of the sample to be measured is on the same time scale as the response function of the system. In these cases, the actual decay may be obtained by deconvolution of the measured signal using an instrumental response function (IRF) generated from a light scattering sample.

TCSPC experiments were carried out using a PicoQuant Fluotime 200 (PicoQuant GmbH, Berlin, Germany) fluorescence lifetime system. Excitation was achieved by means of picosecond diode lasers or LEDs (PicoQuant, 10 MHz repetition rate) and the counting frequency was always below 1%. Desired wavelength was selected by a monochromator (model 9055, Science Tech Inc., London, Canada) and an UV/Vis photomultiplier (model H5783-P01, Hamamatsu Photonics, Japan), sensitive from 175 to 900 nm, was used to detect the fluorescence. Singlet state lifetimes were determined using the PicoQuant FluoFit 4.0 data analysis software.

Method

Singlet lifetime (τ_s)

A solution of the sample in the proper solvent was prepared ensuring that the absorbance of the sample was less than 0.05 in the overlap region between absorption and emission to avoid inner filter effects. The deconvolution of the TCSPC fluorescence signal with the IRF signal – reference sample (Ludox® in water) that directs a small fraction of the excitation light into the detection path - yields the singlet lifetime.

2.2.2. Time-resolved NIR phosphorescence detection (TRPD)

This technique is commonly used for directly and specifically monitoring the formation and decay of single oxygen ($^1O_2$, $O_2(a^1\Delta_g)$), the measurement of its lifetime (τ_Δ) and its quantum yield of formation (Φ_Δ) [2] . It is based on the detection of the weak $^1O_2$ phosphorescence, centered at 1275 nm.

The $^1O_2$ phosphorescence was detected using a customized PicoQuant Fluotime 200 system (Fig. 2.2). A diode-pumped pulsed Nd:YAG laser (FTSS355-Q, Crystal Laser, Berlin, Germany) working at 10 kHz repetition rate and emitting either at 355 nm (5 mW, 0.5 μJ per pulse) or 532 nm (10 mW, 1 μJ per pulse) was used for excitation. A

1064 nm rugate notch filter (Edmund Optics, York, UK) was placed at the exit port of the laser to remove any residual component of its fundamental emission in the near-IR

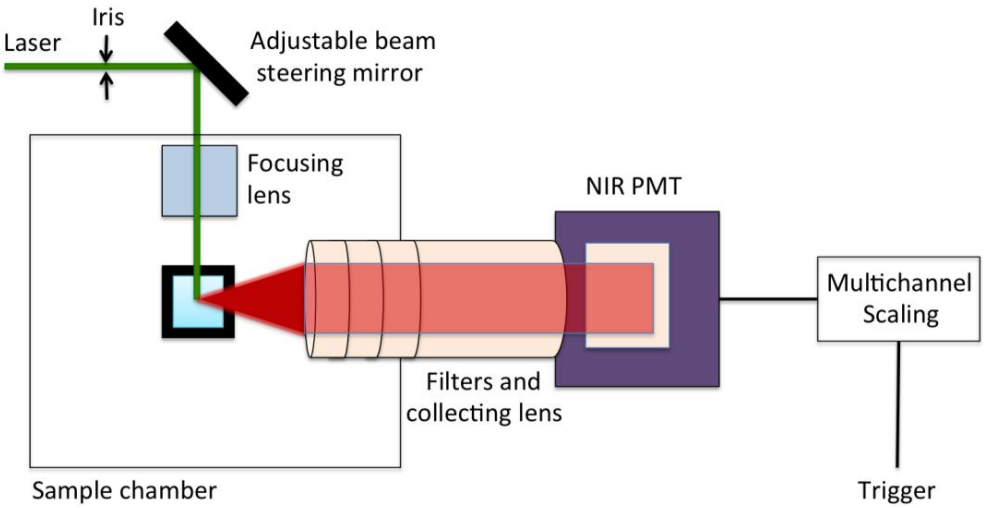

Figure 2.2. Experimental set-up for the photon counting time resolved singlet oxygen phosphorescence detection.

region. The luminescence exiting from the cuvette or solid sample was passed through a cold mirror and a series of long-pass filters of increasing cut-off wavelengths (CVI Melles Griot, Alburquerque, NM) to remove any scattered laser irradiation, and filtered by suitable interference filters to isolate $^1O_2$ emission. A TE-cooled Hamamatsu NIR photomultiplier (model H9170-45, Hamamatsu Photonics, Japan), sensitive from 950 to 1400, was used to detect the conditioned NIR luminescence. The detector was operated in photon counting mode and its output sent to a PicoQuant Nanoharp 250 multichannel scaler. The count histograms were built up until a sufficient signal-to-noise ratio was attained. Data was processed using the PicoQuant FluoFit 4.0 software.

Methods

Photosensitizer's triplet lifetime (τ_T) and $^1O_2$ lifetime (τ_Δ)

Singlet oxygen lifetime was obtained by fitting Eq. 2.2 to the signal detected at 1275 nm,

$$S(t) = S(0) \cdot \frac{\tau_\Delta}{\tau_\Delta - \tau_T} \cdot (e^{-t/\tau_\Delta} - e^{-t/\tau_T}) \qquad (2.2)$$

where *S(0)* is the zero-time amplitude of the signal and τ_T and τ_Δ are the actual lifetimes of the photosensitizer triplet state and singlet oxygen, respectively. Photosensitizer's lifetime was determined, if possible, by fitting Eq. 2.3 to the signal obtained at a wavelength where the triplet state of the photosensitizer emits,

$$[^3PS]_t = K_1 \cdot e^{-t/\tau_T} \qquad (2.3)$$

where K_1 reflects the concentration of triplet excited states of the photosensitizer and τ_T is the actual lifetime of the photosensitizer triplet state.

Quantum yield of $^1O_2$ formation (Φ_Δ)

The quantum yield of singlet oxygen photosensitization is defined as the number of photosensitized $^1O_2$ molecules per absorbed photon. The pre-exponential factor *S(0)*, which is proportional to Φ_Δ, was determined by fitting Eq. 2.2 to the time-resolved phosphorescence intensity at 1275 nm. The quantum yields of $^1O_2$ production were determined from the comparison of *S(0)* to that produced by an optically matched reference in the same solvent and at the same excitation wavelength and intensity (Eq. 2.4) [2] .

$$\Phi_\Delta(\text{sample}) = \frac{S(0)_{sample}}{S(0)_{ref}} \cdot \Phi_\Delta(\text{ref}) \qquad (2.4)$$

Quenching of $^1O_2$ lifetime

Stern-Volmer analysis was used to calculate reaction rate constants (k_Q) form time-resolved data, by means of Eq. 2.5:

$$1/\tau = 1/\tau_0 + k_Q[\text{Q}] \qquad (2.5)$$

where τ and τ_0 are the lifetimes of the reacting species in the presence and absence of a quencher Q, respectively.

2.2.3. UV-Vis nanosecond laser flash photolysis

Transient absorption experiments in the UV-Vis region were carried out using a home-built nanosecond laser flash photolysis system. In this instrument, the 2nd harmonic

(532 nm) or the 3rd harmonic (355 nm) of a Q-switched Nd:YAG laser (Surelite I-10, Continuum) was directed with right-angle geometry to irradiate the sample (10 Hz, 5 ns pulsewidth, 1-10 mJ per pulse). Changes in the sample absorbance were detected using a Hamamatsu R928 photomultiplier to monitor the intensity variation of an analyzing beam produced by a 75 W short-arc Xe lamp (PTI, Birmingham, NJ) and spectral discrimination was obtained using a dual-grating monochromator (mod. 101, PTI). The signal was fed to a Lecroy Wavesurfer 454 oscilloscope for digitizing and averaging (typically 10 shots) and finally transferred by a GPIB interface (National Instruments) to a PC computer for data storage and analysis. A Si photodiode (Laser-Optotronic BPX 65) capturing a reflection of the laser beam was used to trigger the oscilloscope. The energy of the laser pulse was varied by neutral density filters and measured with a pyroelectric energymeter (RJP 735, Laser Precision Corp.). The system was controlled by software developed in our laboratory.
A schematic representation of our set-up is depicted in Fig. 2.3:

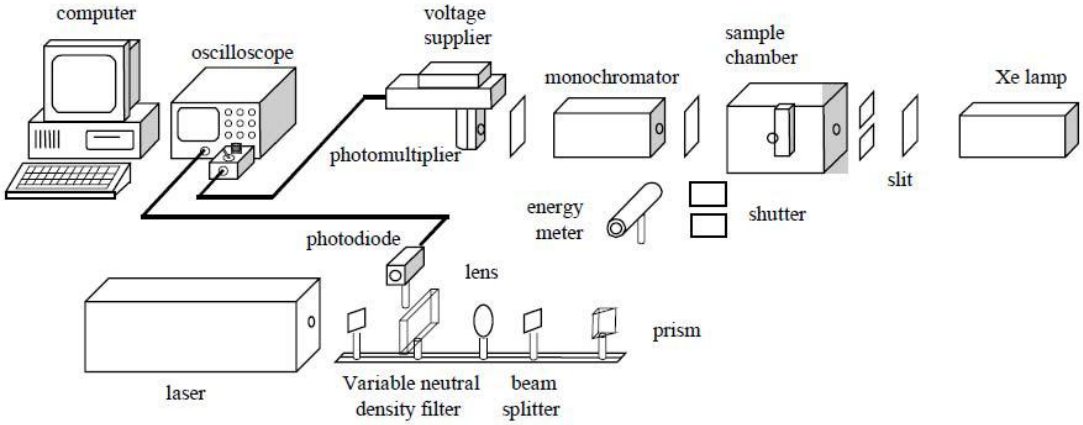

Figure 2.3. Experimental set-up for nanosecond UV-Vis laser flash photolysis.

2.3. LIPOSOME PREPARATION AND CHARACTERIZATION

2.3.1. Liposome preparation

Liposomes used in chapters 4-6 were prepared by microemulsification or extrusion following standard procedures [3,4] .

Method of microemulsification

Lipid mixtures containing the photosensitizer were evaporated to dryness from a chloroform solution and kept in a vacuum desiccator for 12 h over P_2O_5 in order to remove the last traces of the solvent. Multilamellar vesicles (MLVs) were prepared by hydration of the dried lipid films by vortexing for 30 min (alternating 30 s periods of heating and 30 s of vortexing) at a concentration of 20 mg lipid/mL of 50 mM imidazole-HCl buffer (pH 7.4) or 10 mM PBS buffer (pH 7.4) at a temperature above the phase transition temperature (T_m). The MLVs dispersion was frozen and thawed (five times), sonicated (bath sonicator, 15 min, $T>T_m$) and microemulsified (EmulsiFlex B3 device, Avestin, Ottawa, Canada). Microemulsification was carried out by pumping the fluid fifteen times through the interaction chamber ($T>T_m$, 200 kPa). Control liposomes were prepared in the same way but without the photosensitizer. The liposomes were stored in the dark at 4 ºC. Subsequent liposome handling procedures were all performed in the dark.

Long-circulating liposomes with a polymer coating and folate-targeted liposomes incorporate the conjugated lipid (PEG_{3000}-DSPE and folate-PEG_{2000}-DSPE respectively) with the initial mixture of lipids.

Method of extrusion

MLVs were prepared as describe above using imidazole-HCl buffer (pH 7.4) for hydration. In order to reduce and control particle size, MLV suspension was repeatedly extruded through different pore-sized polycarbonate membranes (Osmonics Inc., Livermore, CA) using an extrusion device from Lipex Biomembranes Inc. (Vancouver, Canada) at temperatures above the transition temperature (T_m) of the lipids and high pressure. Liposomes were then incubated for 30 min at $T>T_m$ for annealing.

2.3.2. Liposome lyophilization

To enhance stability during storage, liposomes were lyophilized using 5% trehalose as cryoprotectant agent.

Method

2 mL of liposomal suspension were placed in 4 mL glass vials and frozen at -80 ºC (liquid nitrogen) during 3-5 hours. Vials were subsequently dried during 24 h at -55 ºC and 0.04 mbar (Freeze Dryer Alpha 1-2/LD, Martin Christ GmbH, Germany). Lyophilized liposomes were rehydrated immediately before the experiments by adding 2 mL of sterile water. The resulted suspension was prewarmed at 60 ºC during 15 min and vortexed for 30 min (alternating 30 s periods of heating/vortexing).

2.3.3. Liposome characterization

Determination of encapsulated photosensitizer

The photosensitizer content in the liposomes was evaluated following standard procedures.

Method

Liposomes were disrupted by the addition of THF or DMSO to an aliquot of the liposomal suspension, free of non-entrapped photosensitizer and the absorbance was measured at λ_{max} of the Soret band. The photosensitizer concentration was determined by comparison with standard curves obtained in the same conditions.

Determination of lipid content

Lipid content was quantified by a colorimetric assay with ammonium ferrothiocyanate according to the method of Stewart [5] .

Method

This colorimetric method is based on the formation of a complex between phospholipid and ammonium ferrothiocyanate that is soluble in chloroform. An aliquot of 10 μL of liposomes is disrupted with 2 mL of chloroform and mixed with 2 mL of 0.1 M

ammonium thiocyanate (NH_4SCN). After shaking with vortex for 1 min, the sample is centrifuged for 5 min at 4000 rpm. The reddish lower layer (chloroform) is removed with a Pasteur pipette and the absorbance is read in Specord 205 (Analytik Jena AG, Jena, Germany) at 470 nm. The phospholipid concentration is determined by comparison to the appropriate calibration curve obtained with known amounts of phospholipid.

Determination of size and polydispersity

The average size and polydispersity of unilamellar vesicles and the zeta potential were determined by photon correlation spectroscopy (PCS). A Zetasizer Nano-ZS (Malvern Instruments, UK) and a 4 mW He-Ne laser (Spectra Physics), at an excitation wavelength of 633 nm, were used. Before measuring, samples were appropriately diluted to avoid multiple scattering.

Stability of formulations

To control the stability of the formulations, the photosensitizer and lipid content in liposomes as well as the average size and polydispersity of the vesicles were also determined after storage up to 7 days. The stability of liposomes was also tested in presence of 10% FBS following the procedure described in [6] .

Method

Liposomal suspensions containing photosensitizer were incubated in buffer with 10% FBS at 37ºC with continuous stirring for different periods of time up to 48 h. After each incubation period, 200 μL of the mixtures were withdrawn and centrifuged at 4000 rpm to eliminate any non-encapsulated photosensitizer, appeared as a result of the disruption of the liposomes due to its interaction with serum components. Then, 1.5 mL of THF or DMSO were added to 50 μL of each supernatant to disrupt the liposomes, liberating the photosensitizer still encapsulated in the liposomes and precipitating the serum components. These samples were centrifuged at 4000 rpm to obtain a clear supernatant and the absorption spectra were recorded.

2.4. CELL CULTURES

2.4.1. Cell lines

Cell lines used in chapters 3 and 5 were Human HeLa cervical adenocarcinoma cell line (ATCC CCL-2) and human lung adenocarcinoma A549 cells (ATCC CCL-185). DBA/2 mastocytoma cell line, P815 (ATCC, TIB-64) [7] and the BALB/c colon adenocarcinoma cell line CT26.CL25 (ATCC, CRL-2639) that expressed a tumor antigen, β-galactosidase [8] were used in chapter 6. Primary normal human dermal fibroblasts (hNDF) used in chapter 7 were kindly provided by Hospital de Oviedo.

Culture conditions

All cell lines are adherent cells and grow up to form cellular monolayers toward confluence after seeding. These cells were cultured at 37 ºC in a humidified sterile atmosphere of 95% air and 5% CO_2, using Dulbecco´s Modified Eagle´s Medium (DMEM) or Roswell Park Memorial Institute (RPMI) supplemented with fetal bovine serum (10% v/v), glucose (4.5 g/L), *L*-glutamine (292 mg/L), streptomycin sulfate (10 mg/L) and potassium penicillin (10000 U/L). CT26.CL25 cells were cultured in constant presence of 500 μg/mL G418 antibiotic in order to maintain constant expression of the β-galactosidase.

Cell lines were maintained frozen in DMEM with 10% DMSO. 1.8 mL CryoTubes™ (Nunc, Nalge Nunc International, IL) were filled with the cell suspension and placed in a cell Cryo 1 ºC Freezing Container (Nalgene, Nalge Nunc International, IL) to be slowly frozen up to -80 ºC at a cooling rate of -1 ºC/min for successful cell cryopreservation. Frozen cells were rapidly transferred to a liquid nitrogen container (-196 ºC) and stored.

2.4.2. Dark toxicity

The photosensitizers' effect on cell viability in the absence of light was determined by the MTT colorimetric assay [9] . This assay detects living but not dead cells and it is based on the reduction of a tetrazolium salt to form a formazan dye. The electrons required by this process are given by the mitochondria of viable cells.

Method

Cells were seeded in 24 or 96-well plates and cultured until 80-85% confluence. They were then incubated in the dark with the photosensitizer for 18 h. After washing with sterile Dulbecco's phosphate-buffered saline (PBS), DMEM containing 0.05 mg/mL 3-[4,5-dimethylthiazol-2-yl]-2,5-diphenyltetrazolium bromide (MTT) was added and incubated for 3 h at 37 ºC. The medium was replaced by DMSO and the absorbance at 550 nm was read on a Bio-Rad Benchmark Plus microplate reader (Bio-Rad, Hercules, CA). Experiments were performed in triplicate.

2.4.3. Cell uptake

The cellular uptake of the studied photosensitizers was determined by fluorescence spectroscopy.

Method

Cells were seeded in 6-well plates and grown toward 80-85% confluence. Cells were incubated in the dark with the appropriate photosensitizer concentration, for different times ranging from 30 min to 30 h. In free folate competition studies in chapter 5, 1 mM folic acid was added to the incubation medium. Afterwards, the medium was discarded and the cells were washed three times with PBS, scrapped and resuspended in 1 mL of 2% sodium dodecyl sulphate (SDS) in Milli-Q water. The resulting suspension was centrifuged at 10,000 rpm for 10 min (Sigma 2-16P centrifuge, angle rotor 24x1.5/2.2 mL). The extent of PS uptake was assessed by comparison between the fluorescence of this supernatant to that of standard solutions under the same conditions. The fluorescence intensity values obtained for each sample were normalized to the number of cells determined by the bicinchoninic acid (BCA) protein assay [10] . MicroBCA protein assay kit was purchased from Pierce Protein Research Products (Rockford, IL) and used according to the product information sheet. Each experiment was repeated twice.

2.4.4. Subcellular localization

Confocal microscopy was used to examine the intracellular localization of photosensitizers taken up after delivery by the different systems.

Method

Cells were grown on 22 mm square coverslips placed into 35 mm culture dishes. They were incubated at 37 ºC for 18 h with DMEM containing the appropriate concentration of the photosensitizer. To confirm the intracellular localization of the photosensitizers, the endocytic compartments of the cells were labeled with the fluoroprobe LysoTracker Green DND-26, MitoTracker Green FM or ER-tracker green (Molecular Probes Invitrogen, Eugene, OR) in the culture medium at 37ºC for 30 min. After labeling, the coverslips were washed with PBS and 5-10 min later an Olympus FV1000, multi-photon confocal microscope was used to image the cells. Quantification of overlap between organelle probes and the photosensitizer were carried out using image processing and analysis (IPA) software from the public domain (ImageJ 1.42; http://rsbweb.nih.gov/ij/index.html) [11] .

2.4.5. Light sources

For the irradiation of cell cultures, it has been used two different light sources. In chapters 3-5, irradiation was carried out with Sorisa Photocare LED (Barcelona, Spain) source with wavelength range of 530 ± 20 nm (59 mW) or 625 ± 20 nm (145 mW). In chapter 6, irradiation was carried out with Lumacare lamp (Newport Beach, CA) fitted with a light guide and a 610-680 nm band-pass filter. The irradiance spectra are illustrated in Fig. 2.4.

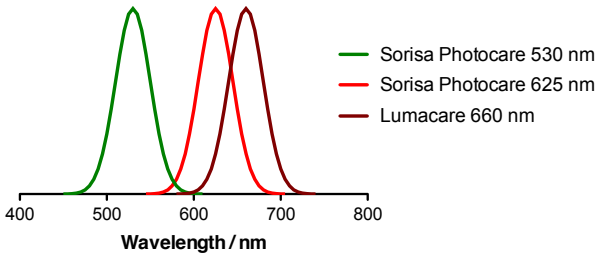

Figure 2.4. Irradiance spectra of the different light sources.

2.4.6. Photodynamic treatments *in vitro*

The photosensitizers' effect on cell viability after delivery of a certain light dose was determined by the MTT colorimetric assay described above.

Method

Cells were seeded in 96-well plates and cultured towards 80-85% confluence. They were then incubated in the dark at 37 ºC with DMEM containing the photosensitizer. After 18 or 24 h incubation, cells were washed three times with PBS and replenish with fresh media. Irradiation was carried out with a Sorisa Photocare LED or Lumacare light sources described above and the light intensity at the irradiation site was measured with a LaserStar Ophir power meter (Logan, UT). Cells were irradiated for different light doses and then incubated for 24 h before the MTT assay for cell viability. Experiments were performed in triplicate.

2.4.7. Spectroscopic measurements of cell suspensions

Spectroscopic measurements were recorded on the systems previously described. Cell suspension samples were prepared using the following method.

Method

Cells were incubated in the dark with the photosensitizer for 18 or 24 h. The medium was discarded and the cells were washed three times with PBS, scrapped or trypsinized and resuspended in 1.5 mL of PBS or D_2O-based PBS (D-PBS). The samples contained about 8 millions of cells in 1.5 mL of PBS and were continuously stirred during the measurements. The measurements were then carried out within the following 45 min.

2.5. ANIMAL MODELS

2.5.1. Animal tumor models

DBA/2 and BALB/c mice (6-8 weeks old) were purchased from Charles River Laboratories (Boston, MA). All experiments were carried out according to a protocol approved by the Subcommittee on Research Animal Care at (Institutional Animal Care and Use Committee) at Massachusetts General Hospital and were in accord with guidelines from the National Institutes of Health (NIH). Mice were inoculated with 350,000 cells subcutaneously into the depilated left thigh. Two orthogonal dimensions (a and b) of the tumor were measured 3-4 times a week with a vernier caliper. Tumor volumes were calculated as $4\pi/3\ [(a+b)/4]^3$. PDT was performed when tumors reached a diameter of 5-7 mm (around 9 days after cell inoculation).

2.5.2. PDT and tumor response

The effects of photosensitizer formulation and targeting strategy on PDT effectiveness *in vivo* were evaluated as follows (Fig. 2.5).

Method

Tumor bearing mice were anaesthetized with an intraperitoneal injection of 87.5 mg/kg of ketamine and 12.5 mg/kg xylazine. Photosensitizer formulation (1 mg/kg) was administrated intravenously via the tail vein injection. 15 min or 24 h after injection of photosensitizer, 660-nm Lumacare light source was used to irradiate a homogeneous spot of 1.5-cm diameter that covered the tumor and a margin of normal tissue. A total fluence of 75 or 150 J/cm^2 was delivered at a fluence rate of 100 mW/cm^2. The mice were sacrificed when any of the tumor diameters exceeded 1.5 cm or when any signs of disseminated metastatic tumor appeared (e.g. >15% loss of body weight).

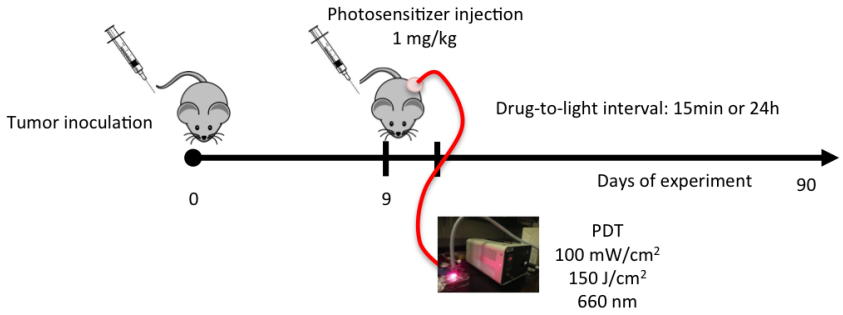

Figure 2.5. Schematic depiction of the steps involved in performing PDT on a tumor model in mice.

2.5.3. *In vivo* fluorescence imaging

Photosensitizer accumulation and photobleaching in tumors were followed by fluorescence imaging.

Method

Tumor bearing mice were anaesthetized and subsequently placed in the light-tight chamber of the CRI Maestro (Caliper Life Sciences, Hopkinton, MA) *in vivo* fluorescence imaging system [12] . The instrument was set up as follows: images were captured every 10 nm throughout the wavelength range 650-800 nm using a 488-nm excitation filter, an LP 515-nm emission filter, and an exposure time of 100 ms. The focus and the stage height were set manually. Mice were imaged at different time points after photosensitizer tail vein injection. After the fluorescence image acquisition, the image cubes were unmixed (deconvolved) using a spectral library containing the autofluorescence of the mice skin and a dilute sample of photosensitizer.

2.5.4. Vascular perfusion

The effects of PDT on tumor vascular perfusion were studied using Hoechst 33342. The fluorescence of Hoechst 33342 is visible only in the functional vessels [13,14] .

Method

Vascular perfusion was assessed 1 h after PDT treatment by Hoechst 33342 injection (40 mg/kg in physiologic saline, i.v.) 1 min before sacrificing the animals by cervical

dislocation under deep anesthesia. After excision, tumors were snap-frozen in liquid nitrogen and stored at -80 ºC until sectioning. Sections of 5 μm thickness were cut from the center of the tumor and examined under a fluorescence microscope (Axiovert, Carl Zeiss Microscopy, Thorwood, NY) with a 340-380-nm bandpass excitation filter and a 430-nm long-pass filter.

2.6. REFERENCES

[1] W. Becker, Advanced Time-Correlated Single Photon Counting Techniques, Springer, Germany, 2005.

[2] S. Nonell, S.E. Braslavsky. Time-resolved singlet oxygen detection, Methods Enzymol. 319 (2000) 37-49.

[3] F. Postigo, M. Mora, M.A. De Madariaga, S. Nonell, M.L. Sagrista. Incorporation of hydrophobic porphyrins into liposomes: characterization and structural requirements, Int. J. Pharm. 278 (2004) 239-254.

[4] F. Postigo, M.L. Sagrista, M.A. De Madariaga, S. Nonell, M. Mora. Photosensitization of skin fibroblasts and HeLa cells by three chlorin derivatives: Role of chemical structure and delivery vehicle, Biochim. Biophys. Acta 1758 (2006) 583-596.

[5] J.C. Stewart. Colorimetric determination of phospholipids with ammonium ferrothiocyanate, Anal. Biochem. 104 (1980) 10-14.

[6] M.L. Sagristà, F. Postigo, M.A.D. Madariaga, R.M. Pinto, S. Caballero, A. Bosch, et al. Photodynamic inactivation of viruses by immobilized chlorin-containing liposomes, J. Porphyrins Phthalocyaines 13 (2009) 578-588.

[7] B. Van den Eynde, B. Lethe, A. Van Pel, E. De Plaen, T. Boon. The gene coding for a major tumor rejection antigen of tumor P815 is identical to the normal gene of syngeneic DBA/2 mice, J. Exp. Med. 173 (1991) 1373-1384.

[8] M. Wang, V. Bronte, P.W. Chen, L. Gritz, D. Panicali, S.A. Rosenberg, et al. Active immunotherapy of cancer with a nonreplicating recombinant fowlpox virus encoding a model tumor-associated antigen, J. Immunol. 154 (1995) 4685-4692.

[9] T. Mosmann. Rapid Colorimetric Assay for Cellular Growth and Survival - Application to Proliferation and Cyto-Toxicity Assays, J. Immunol. Methods 65 (1983) 55-63.

[10] R.E. Brown, K.L. Jarvis, K.J. Hyland. Protein measurement using bicinchoninic acid: elimination of interfering substances, Anal. Biochem. 180 (1989) 136-139.

[11] M. Alvarez, A. Villanueva, P. Acedo, M. Canete, J.C. Stockert. Cell death causes relocalization of photosensitizing fluorescent probes, Acta Histochem. 113 (2011) 363-368.

[12] P. Mroz, Y.Y. Huang, A. Szokalska, T. Zhiyentayev, S. Janjua, A.P. Nifli, et al. Stable synthetic bacteriochlorins overcome the resistance of melanoma to photodynamic therapy, FASEB J. 24 (2010) 3160-3170.

[13] M. Triesscheijn, M. Ruevekamp, M. Aalders, P. Baas, F.A. Stewart. Outcome of mTHPC mediated photodynamic therapy is primarily determined by the vascular response, Photochem. Photobiol. 81 (2005) 1161-1167.

[14] B. Chen, B.W. Pogue, P.J. Hoopes, T. Hasan. Combining vascular and cellular targeting regimens enhances the efficacy of photodynamic therapy, Int. J. Radiat. Oncol. Biol. Phys. 61 (2005) 1216-1226.

Chapter 3

Towards the ideal photosensitizer

Characterization of new porphycenes

In this chapter, the photophysical properties of a group of new porphycene-based photosensitizers are determined. Among the photosensitizers tested, temocene, the porphycene analogue to temoporfin, shows the greatest potential for photodynamic therapy. Compared to temoporfin, temocene is endowed with 2.5-fold larger absorption coefficient in the red part of the spectrum while keeping its excellent photophysical and singlet oxygen photosensitization ability. While its photodynamic activity towards HeLa cells is lower than that of temoporfin, its higher photostability, lower dark toxicity and mitochondrial localisation make temocene a promising candidate for photodynamic therapy applications.

3.1. INTRODUCTION

During the last two decades a substantial effort has been put into the development and scrutiny of the second-generation photosensitizers (PSs) [1-4] since no single PS has yet been found to meet all the demands for successful application in oncology. Amongst these second generation PSs, a series of derivatives of *m*-tetrahydroxyphenyl porphyrin (*m*-THPP) have been particularly promising [5,6]. The hydroxyl functions modulate the hydrophobic character of the macrocyclic core and therefore its solubility, and provide hydrogen bonding capability for specific interactions with receptor sites. One of the most active photosensitizers is *m*-tetrahydroxyphenyl chlorin (*m*-THPC, temoporfin) [7-9]. Although temoporfin is currently approved for photodynamic therapy (PDT) treatment of head and neck cancer under the trade name Foscan® [10,11], this PS is not without its own shortcomings due to its high potency and prolonged skin sensitivity [12,13].

Amongst the porphyrin-based photodynamic therapy agents, porphycenes show better absorption properties than their structural isomers [14,15] owing to the lower molecular symmetry. The absorption on the red part of the spectrum, where the tissues are more transparent to light [16], the demonstrated cell photoinactivation [17-20] and the little photosensitivity associated [21] placed the porphycenes in an excellent position as promising candidates for PDT treatments. Since the synthesis of the first porphycene in 1986 [22], a variety of substituted derivatives have been prepared [23] but the long and complex syntheses involved were a limiting factor until very recently.

This chapter shows our contribution to the development of new porphycenes in order to find the optimal PS for PDT applications. In the light of the challenge set by Bonnett [24], who suggested the investigation of the corresponding *m*-tetra(hydroxyphenyl) porphycene derivative, we report on the photophysics, subcellular localization, and photodynamic activity of the porphycene analogue of temoporfin, which we term *temocene*. The photophysical properties of its precursor (*m*-tetra(isopropoxyphenyl) porphycene) and its palladium complex are also reported. Moreover, we studied the effect of carboxylate groups in the solubility and properties of the PS.

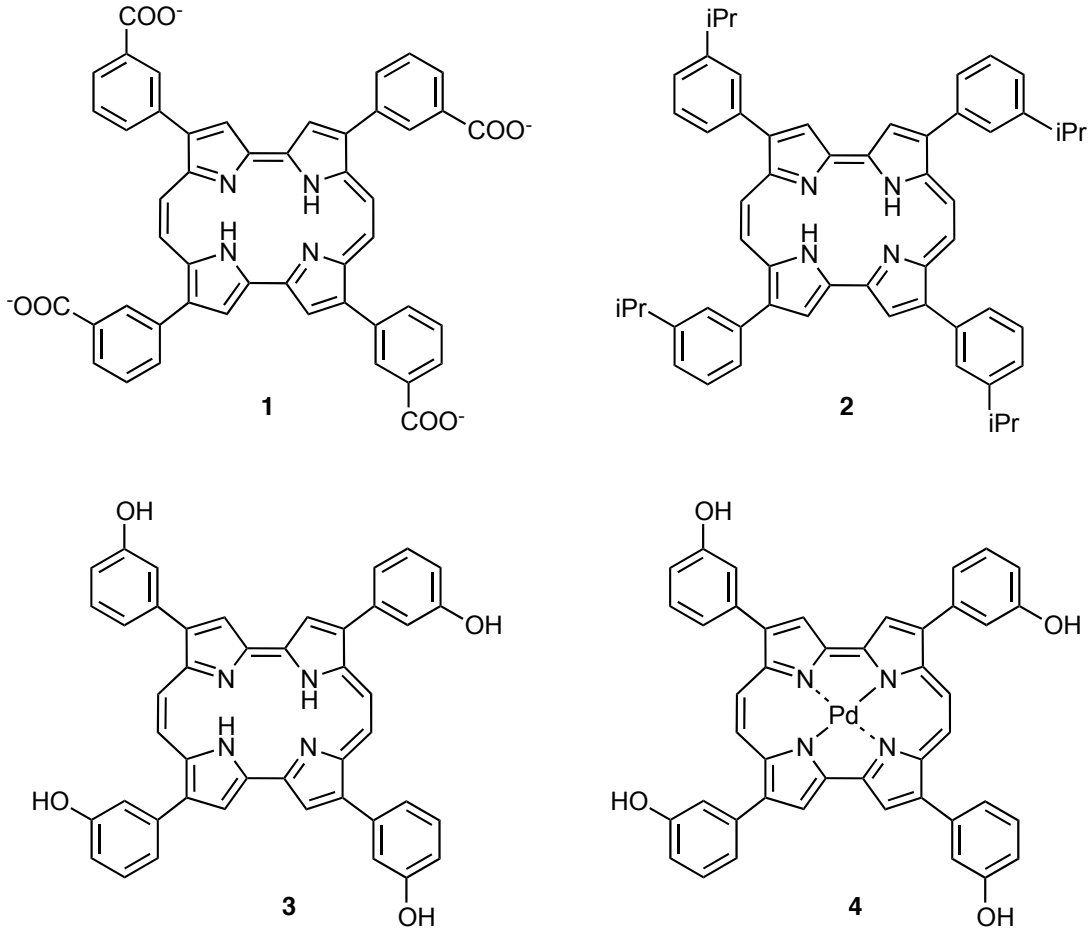

Figure 3.1. Chemical structures of pophycenes characterized in this chapter. **1**. 2,7,12,17-(3-carboxylatophenyl) porphycene, *m*-TCPPo; **2.** 2,7,12,17-(3-isopropoxyphenyl) porphycene, iPrOTPPo; **3.** 2,7,12,17-(3-hydroxyphenyl) porphycene; *m*-THPPo **4.** Palladium(II)-2,7,12,17-(3-hydroxyphenyl) porphycene, PdTPPo.

3.2. EXPERIMENTAL SECTION

Liquid chromatography conditions. Liquid Chromatography (HPLC) was performed with a HP 1090 series liquid chromatograph equipped with a diode array detector. *m*-THPPo was analyzed on a 30 mm x 4 mm, 3 mm particle, Lichrocart Purospher STAR RP-18E column. Detection was achieved at 375 nm. All chromatography runs were performed at room temperature with a mobile phase flow rate of 1.0 mL min^{-1}. Isocratic elution was performed with 77:23 ACN/H_2O.

Photobleaching studies. Optically-matched solutions of *m*-THPC or *m*-THPPo in acetone were irradiated with a Q-switched Nd-YAG laser (Surelite I-10, Continuum) tuned to 532 nm. At intervals the cuvette was removed and the spectrum in the range of 450-800 was recorded in order to follow the course of photobleaching.

Light dose and concentration dependence phototoxicity. HeLa cells were seeded in 24-well plates and cultured towards 80-85% confluence. They were then incubated in the dark at 37 ºC with serum-free DMEM containing 1-10 μM *m*-THPPo in DMSO. After 18 h incubation, cells were washed three times with PBS and replenish with fresh DMEM. Irradiation was carried out with Sorisa Photocare LED source with wavelength range of 620-645nm. The light intensity at the irradiation site was 24 mW/cm^2, measured with a LaserStar Ophir power meter. Cells were irradiated for different light doses and then incubated for 24 h before the MTT assay for cell viability. Experiments were performed in quadruplicate.

Effect of ROS quenchers in temocene-induced phototoxicity. HeLa cells were seeded in 24-well plates and cultured towards 80-85% confluence. They were then incubated in the dark at 37 ºC with serum-free DMEM containing 1 μM *m*-THPPo in DMSO. After 18 h incubation, cells were washed three times with PBS and incubated for 10 min with fresh DMEM containing D-mannitol (0.4 or 40 mM) as hydroxyl radical quencher or sodium azide (0.5 or 5 mM) as singlet oxygen scavenger. 5 J/cm^2 light dose was delivered and cells were then incubated for 24 h before the MTT assay for cell viability. Experiments were performed in quadruplicate.

.

3.3. RESULTS AND DISCUSSION

Physical and photophysical properties. The photophysical properties of the tetraphenylporphycenes studied are discussed in detail in the following sections. A summary is given in Table 3.1.

Table 3.1. Summary of photophysical properties of the porphycenes studied

	m-TCPPo (MeOH/H_2O)	iPrOTPPo (Benzene)	*m*-THPPo (THF)	PdTPPo (THF)
λ_{max}/nm	649/627	659	656	630
/$M^{-1}cm^{-1}$	n.d.	57000	69100	78000
λ_F/nm	662,717/655,720	670,735	666,729	n.a.
Φ_F	0.079/0.002	0.1	0.084	n.a.
τ_S/ns (Air)	n.d.	3.8	2.3	n.a.
τ_T/ s (Ar)	n.d.	n.d.	260	10
k_q^{O2}/$M^{-1}s^{-1}$	n.d.	n.d.	$2.1 \cdot 10^9$	n.d.
Φ_Δ	0.07/-	0.19	0.1	0.62

λ_{max}, maximum of the lowest-energy absorption band; e, absorption coefficient at λ_{max}; λ_F, maximum of the emission bands; Φ_F, fluorescence quantum yield; τ_S, singlet state lifetime; τ_T, triplet excited state lifetime; k_q^{O2}, rate constant for triplet quenching by ground-sate oxygen; Φ_Δ, singlet oxygen quantum yield.

n.d. not determined

n.a. not applied

m-tetra(carboxylatophenyl) porphycene (*m*-TCPPo): a water-soluble porphycene

One of the major drawbacks of the second-generation PSs is their poor solubility in aqueous environment. An attempt to solve this problem is to endow the hydrophobic core with carboxylate groups. As observed in Fig. 3.2, *m*-TCPPo shows the typical porphycene absorption spectrum in MeOH, with three bands in the red range of the spectrum. The spectrum in water loses much of the structure, indicating not

surprisingly that aggregation is occurring in aqueous media despite the four negative charges.

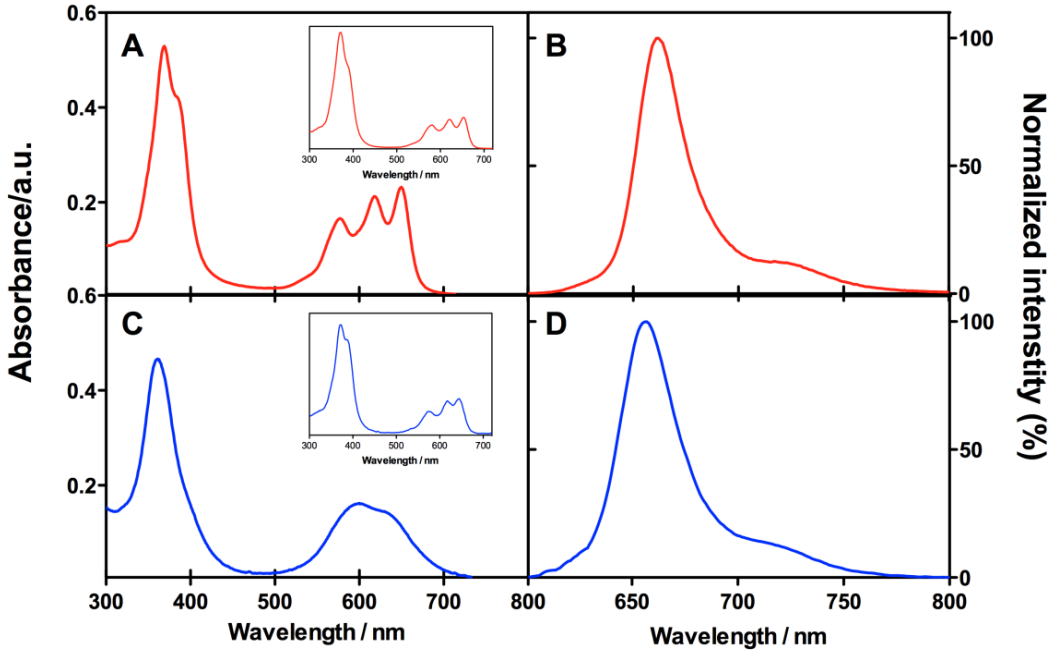

Figure 3.2. (A,C) Absorption and (B,D) fluorescence spectrum of *m*-(tetracarboxylatophenyl) porphycene in (A,B) MeOH and (C,D) water. Insets: Excitation spectra of the fluorescence at 730 nm.

However, both in water and in MeOH, the fluorescence spectra match the typical fluorescence spectrum of porphycenes, with a main band and a weaker shoulder at lower energies that mirror the S1 ← S0 absorption transition [15]. Interestingly, the excitation spectrum matches in all cases the absorption spectrum of the monomer, indicating that the aggregates are not emissive. The fluorescence quantum yield, Φ_F, was 0.079 ± 0.005 in MeOH, and 0.002 ± 0.005 was found in water.

The singlet oxygen production quantum yield, Φ_Δ, was determined by means of its phosphorescence at 1275 nm. Φ_Δ value of 0.07 ± 0.02 was determined in MeOH upon excitation of 532 nm. In aqueous media aggregation strongly prevents its photosensitizing ability. These results fully agree with the water-soluble tricationic porphycene recently studied in our group [25].

_m_-tetra(hydroxyphenyl) porphycene (_m_-THPPo) and _m_-tetra(isopropoxyphenyl) porphycene (_m_-iPrOPPo): the temocene and its precursor

As observed in Fig. 3.3, *m*-THPPo showed the typical absorption spectrum of free-base porphycenes, with three intense bands in the red part of the spectrum showing a maximum absorption coefficient of ca. 70,000 M^{-1} cm^{-1} at 656 nm, 2.5-fold higher than that of temoporfin [6]. The fluorescence emission spectrum also matched the typical fluorescence spectrum of porphycenes, with a main band at 666 nm and a weaker shoulder at lower energies that mirror the S1←S0 absorption transition [15]. *m*-iPrOTPPo showed no significant differences in the absorption and emission properties (see Table 3.1). The fluorescence quantum yield was Φ_F = 0.084 ± 0.005 for *m*-THPPo and Φ_F = 0.1 ± 0.02 for *m*-iPrOTPPo, suggesting that both temocene and its precursor could be used also for fluorescence diagnostic purposes.

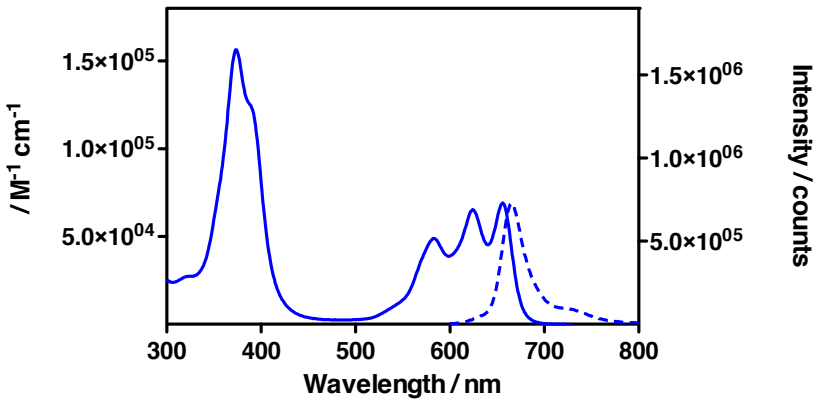

Figure 3.3. Absorption (solid line) and emission (dotted line) spectra of *m*-THPPo in THF.

The excited singlet state decayed with lifetime 2.3 ± 0.1 ns for *m*-THPPo (Fig. 3.4) and 3.8 ± 0.1 ns for *m*-iPrOTPPo. The newborn triplet state lived 260 μs in argon-saturated solutions, long enough to provide for rich photochemistry (Fig. 3.5).

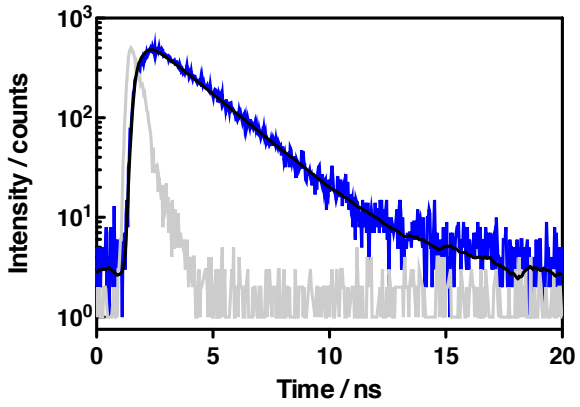

Figure 3.4. Fluorescence decay of *m*-THPPo in THF(λ_{exc}= 375 nm, λ_{em}= 660 nm).

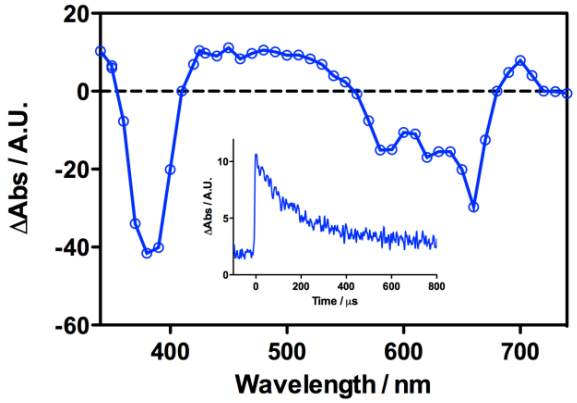

Figure 3.5. Triplet-minus-singlet absorption spectrum of *m*-THPPo in argon-saturated acetone. Inset: Transient decay at 490nm.

Indeed, temocene was able to photosensitize the production of singlet oxygen ($^1O_2$) in aerated solutions. The quantum yield, Φ_Δ = 0.10 ± 0.01, was high enough to expect substantial phototoxicity to cells. The quantum yield for its precursor *m*-iPrOTPPo was Φ_Δ = 0.19 ± 0.02.

As shown in Fig. 3.6 the rate constant for triplet decay ($1/\tau_T$) increased linearly with the concentration of oxygen, yielding a quenching rate constant of 2.1 x 10^9 M^{-1} s^{-1} for temocene.

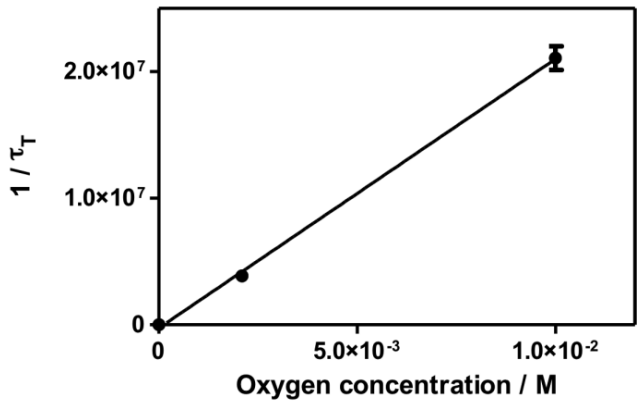

Figure 3.6. Stern-Volmer plot of $1/\tau_T$ at different oxygen concentrations in THF.

The kinetics of temocene and temoporfin photobleaching under the same irradiation conditions were comparatively shown in Fig. 3.7. Temocene was substantially more photostable than temoporfin.

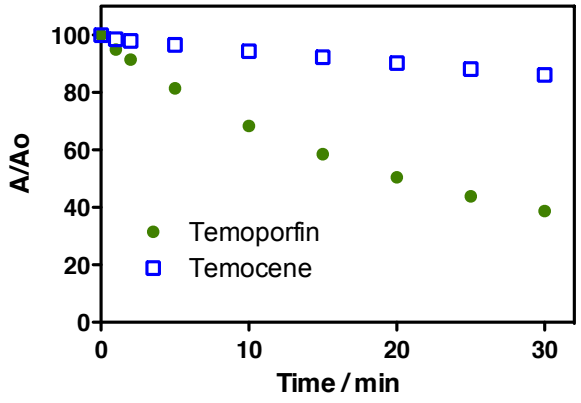

Figure 3.7. Photobleaching of temoporfin and temocene solutions in aerated acetone upon irradiation with 532-nm laser pulses. Absorbance values were recorded at 656 and 650 nm, respectively.

Palladium(II)-2,7,12,17-(3-hydroxyphenyl) porphycene (PdTHPPo)

The absorption spectrum of PdTPPo is shown in Fig. 3.8. Compared to *m*-THPPo the three Q-bands were reduced to two as a result of the increase of symmetry. The lowest-energy Q-band suffered a hypsochromic shift reflecting electron donation from the metal into the pophycene, thus raising their energy. The presence of metal also led

to an increase in the absorption coefficient of the lowest energy Q-band. These observations agree with the photophysical properties of metalloporphycenes in general [26].

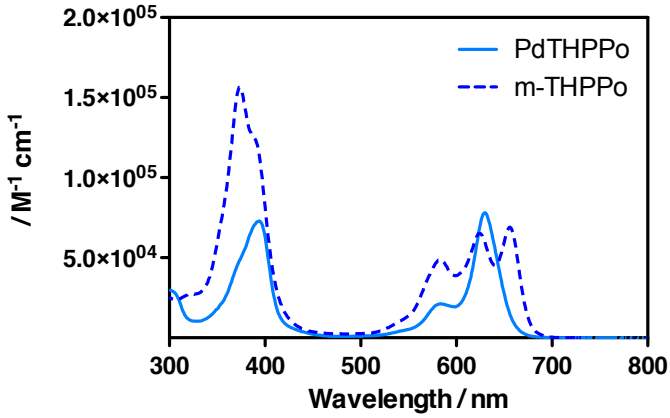

Figure 3.8. Absorption spectra of PdTHPPo (solid line) and *m*-THPPo (dotted line) in THF.

PdTHPPo did not show fluorescence, an analogous situation to that found for PdTPPo [26]. This reflects an enhancement of the intersystem crossing probability owing to the heavy-atom effects.

The triplet PdTHPPo decayed with monoexponential kinetics with a lifetime of 10 μs in acetone (Fig. 3.9), much shorter to that of *m*-THPPo. In spite of this fact, it was still long enough to be deactivated by oxygen, yielding a Φ_{Δ} = 0.62 ± 0.05.

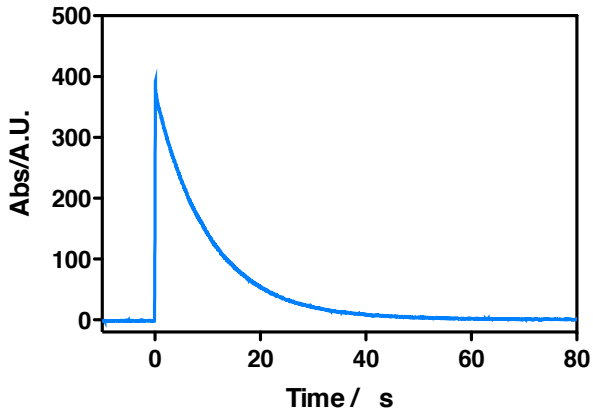

Figure 3.9. Transient absorption of triplet PdTHPPo in argon-saturated acetone (λ_{exc}=355 nm, λ_{em}=490 nm).

In the light of the promising results obtained for *m*-THPPo, the synthetic availability and its analogy to temoporfin, one of the PS clinically approved, we decided to test its *in vitro* photodynamic activity.

Photosensitization experiments. Studies on the dark- and phototoxicity of temocene and temoporfin are summarized in Fig. 3.10. HeLa cells were incubated in the dark with different concentrations of *m*-THPPo or *m*-THPC in DMSO for 18 h prior to photosensitization.

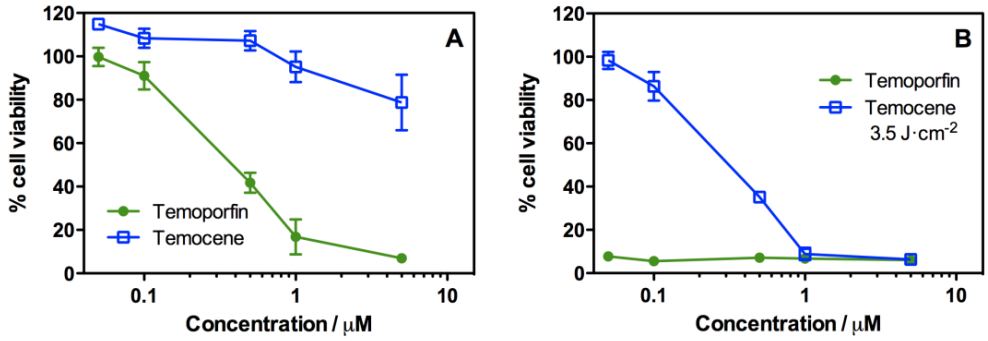

Figure 3.10. Viability of HeLa cells measured by the MTT assay after 18 h incubation with different concentrations of *m*-THPPo or *m*-THPC in DMSO. (A) Dark toxicity. (B) Photodynamic induced cytotoxicity after 3.5 J·cm^{-2}. Mean ± SD from at least four independent experiments are shown.

A 3-(4,5-dimethylthiazol-2-yl)-2,5-diphenyltetrazolium bromide (MTT) assay [27] was performed 24 h after treatment to establish the *m*-THPPo and *m*-THPC dark toxicity. Our studies show that temocene is substantially less toxic in the dark than temoporfin, which is advantageous for its therapeutic applications. The photodynamic damage on HeLa cells was assessed after delivery of different light doses from a LED source at 625 nm. Complete cell inactivation could be achieved at light doses of just 3.5 J·cm^{-2} using *m*-THPPo concentrations higher than 5 μM. At higher light doses the same result could be obtained at concomitantly lower temocene concentrations.

Effect of ROS quenchers on cell phototoxicity. To determine which ROS is predominantly involved in cell death, the phototoxicity of temocene to HeLa cells was evaluated in the presence of ROS inhibitors, namely D-mannitol (0.4 and 40 mM) as an HO• quencher and sodium azide (0.5 and 5 mM) as a $^1O_2$ scavenger. Fig. 3.11. shows dose-dependent inhibitory effects of D-mannitol and sodium azide. The phototoxicity of temocene was partially quenched by sodium azide but not by D-mannitol suggesting that singlet oxygen is the mainly responsible for cell cytotoxicity.

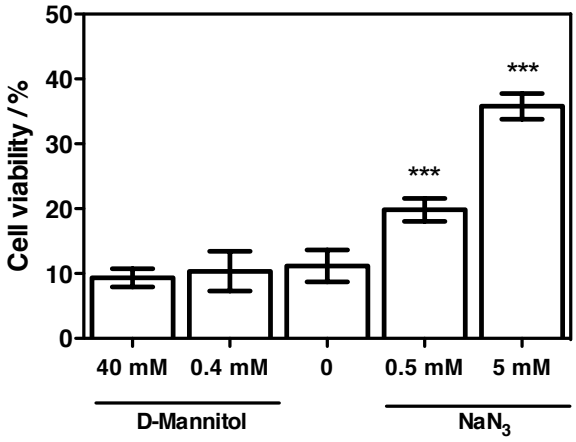

Figure 3.11. Cell survival (%) of HeLa cells treated with 1 μM temocene in the absence of ROS quenchers and in the presence of sodium azide (NaN3, 1O2 quencher) or D-mannitol (HO• radical scavenger) after 5 J/cm^2 light dose. Mean ± SD from at least four independent experiments are shown. *** $p < 0.001$ vs no ROS quenchers.

Subcellular localization by fluorescence microscopy. Fluorescence micrographs of HeLa cells after 18 h incubation with temocene are shown in Fig. 3.12. Cells incubated with 0.5 μM *m*-THPPo showed a fluorescence pattern similar to that of control cells. With 1 μM and especially 10 μM *m*-THPPo, a red fluorescence could be distinguished, which colocalized with the blue mitochondrial autofluorescence and with the green emission from MitoTracker®Green (Fig. 3.12A and merged image 3.12C), indicating that mitochondria are the main sites of temocene accumulation. This is fortunate as this organelle is one of the most attractive PDT targets for triggering apoptosis [28-30]. In addition, a diffuse red fluorescence could be detected in the cytoplasm. No relocalization of the PS was observed when cells were exposed to prolonged irradiation.

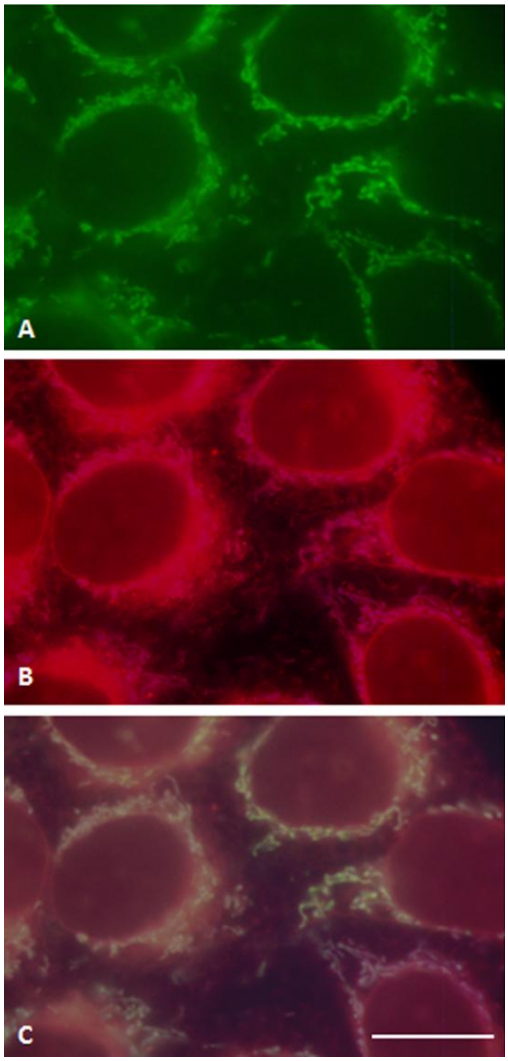

Figure 3.12. Fluorescence microscopy images of living HeLa cells incubated with MitoTracker®Green for 30 min, followed by 18 h 10 μM DMSO-loaded *m*-THPPo. (A) Cells observed under blue excitation. (B) Cells observed under UV excitation. (C) Merged image. Scale bar: 20 μm.

3.4. CONCLUSIONS

In summary, we have reported the photophysical properties of a collection of new porphycene-base PSs. The introduction of carboxylate groups in the periphery of the PS core enhances its aqueous solubility although aggregation is not avoided in this environment. However, the monomeric porphycene is a far worse PS than the parent TPPo. The introduction of metals in the porphycene macrocycle induces a hyperchromic effect in the lowest energy Q-band and high singlet oxygen formation quantum yield. The results of these studies provide clues for improving the design of novel PS based on the porphycene macrocycle.

We also have characterized temocene, a porphycene analogue to temoporfin. Its excellent photophysical properties, mitochondrial localization, and, above all, its photodynamic efficiency, make temocene a promising candidate for antitumoral photodynamic therapy. Compared to temoporfin, temocene shows lower activity but also lower dark toxicity and superior photostability. Taken together, temocene is endowed with potential value for photodynamic treatments and is worth of further studies. Development of a liposome-based formulation of temocene for its improved cell delivery and *in vivo* photodynamic activity is described in the following chapters.

3.5. REFERENCES

[1] M.J. Garland, C.M. Cassidy, D. Woolfson, R.F. Donnelly. Designing photosensitizers for photodynamic therapy: strategies, challenges and promising developments, Future Med. Chem. 1 (2009) 667-691.

[2] A.E. O'Connor, W.M. Gallagher, A.T. Byrne. Porphyrin and nonporphyrin photosensitizers in oncology: preclinical and clinical advances in photodynamic therapy, Photochem. Photobiol. 85 (2009) 1053-1074.

[3] L.B. Josefsen, R.W. Boyle. Photodynamic therapy and the development of metal-based photosensitisers, Metal-based drugs (2008) 1-24.

[4] S.B. Brown, E.A. Brown, I. Walker. The present and future role of photodynamic therapy in cancer treatment, Lancet Oncol. 5 (2004) 497-508.

[5] R. Bonnett, R.D. White, U.J. Winfield, M.C. Berenbaum. Hydroporphyrins of the meso-tetra(hydroxyphenyl)porphyrin series as tumour photosensitizers, Biochem. J. 261 (1989) 277-280.

[6] R. Bonnett, P. Charlesworth, B. Djelal D., S. Foley, D. McGarvey J., T. George Truscott. Photophysical properties of 5,10,15,20-tetrakis(m-hydroxyphenyl)porphyrin (m-THPP), 5,10,15,20-tetrakis(m-hydroxyphenyl)chlorin (m-THPC) and 5,10,15,20-tetrakis(m-hydroxyphenyl)bacteriochlorin (m-THPBC): a comparative study, J. Chem. Soc., Perkin Trans. 2. (1999) 325-328.

[7] Q. Peng, J.H. Moan, L.W. Ma, J.M. Nesland. Uptake, Localization, and Photodynamic Effect of Meso-Tetra(hydroxyphenyl)porphine and its Corresponding Chlorin in Normal and Tumor-Tissues of Mice Bearing Mammary-Carcinoma, Cancer Res. 55 (1995) 2620-2626.

[8] L. Morlet, V. Vonarx-Coinsmann, P. Lenz, M. Foultier, L.X. de Brito, C. Stewart, et al. Correlation between meta(tetrahydroxyphenyl)chlorin (m-THPC) biodistribution and photodynamic effects in mice, J. Photochem. Photobiol. B: Biol. 28 (1995) 25-32.

[9] M. Triesscheijn, M. Ruevekamp, M. Aalders, P. Baas, F.A. Stewart. Outcome of mTHPC mediated photodynamic therapy is primarily determined by the vascular response, Photochem. Photobiol. 81 (2005) 1161-1167.

[10] M.G. Dilkes, M.L. DeJode, A. RowntreeTaylor, J.A. McGilligan, G.S. Kenyon, P. McKelvie. m-THPC photodynamic therapy for head and neck cancer, Lasers Med. Sci. 11 (1996) 23-29.

[11] S. Banfi, E. Caruso, S. Caprioli, L. Mazzagatti, G. Canti, R. Ravizza, et al. Photodynamic effects of porphyrin and chlorin photosensitizers in human colon adenocarcinoma cells, Bioorg. Med. Chem. 12 (2004) 4853-4860.

[12] A.M. Ronn, M. Nouri, L.A. Lofgren, B.M. Steinberg, A. Westerborn, T. Windahl, et al. Human tissue levels and plasma pharmacokinetics of temoporfin (Foscan(R), mTHPC), Lasers Med. Sci. 11 (1996) 267-272.

[13] R.K. Pandey. Recent advances in photodynamic therapy, J. Porphyrins Phthalocyanines. 4 (2000) 368-373.

[14] P.F. Aramendia, R.W. Redmond, S. Nonell, W. Schuster, S.E. Braslavsky, K. Schaffner, et al. The photophysical properties of porphycenes: potential photodynamic therapy agents, Photochem. Photobiol. 44 (1986) 555-559.

[15] J.C. Stockert, M. Cañete, A. Juarranz, A. Villanueva, R.W. Horobin, J.I. Borrell, et al. Porphycenes: facts and prospects in photodynamic therapy of cancer, Curr. Med. Chem. 14 (2007) 997-1026.

[16] G. Jori. Far-red-absorbing photosensitizers: their use in the photodynamic therapy of tumours, J. Photochem. Photobiol. A:Chem. 62 (1992) 371-378.

[17] M. Guardiano, R. Biolo, G. Jori, K. Schaffner. Tetra-n-propylporphycene as a tumour localizer: pharmacokinetic and phototherapeutic studies in mice, Cancer Lett. 44 (1989) 1-6.

[18] M. Cañete, M. Lapena, A. Juarranz, V. Vendrell, J.I. Borrell, J. Teixido, et al. Uptake of tetraphenylporphycene and its photoeffects on

actin and cytokeratin elements of HeLa cells, Anticancer Drug Des. 12 (1997) 543-554.

[19] A. Villanueva, M. Cañete, S. Nonell, J.I. Borrell, J. Teixido, A. Juarranz. Photodamaging effects of tetraphenylporphycene in a human carcinoma cell line, Anticancer Drug Des. 11 (1996) 89-99.

[20] M. Cañete, C. Ortega, A. Gavalda, J. Cristobal, A. Juarranz, S. Nonell, et al. Int. J. Oncol. 24 (2004) 1221-1228.

[21] C. Abels, R.-. Szeimies, P. Steinbach, C. Richert, A.E. Goetz. Targeting of the tumor microcirculation by photodynamic therapy with a synthetic porphycene, J. Photochem. Photobiol. B: Biol. 40 (1997) 305-312.

[22] E. Vogel, M. Kocher, H. Schmickler, J. Lex. Porphycene - a Novel Porphin Isomer, Angew.Chem.-Int.Edit.Engl. 25 (1986) 257-259.

[23] C. Richert, J.M. Wessels, M. Muller, M. Kisters, T. Benninghaus, A.E. Goetz. Photodynamic antitumor agents: beta-methoxyethyl groups give access to functionalized porphycenes and enhance cellular uptake and activity, J. Med. Chem. 37 (1994) 2797-2807.

[24] R. Bonnett, Chemical Aspects of Photodynamic Therapy (Advanced Chemistry Texts, V. 1), CRC 2000.

[25] X. Ragàs, D. Sánchez-García, R. Ruiz-González, T. Dai, M. Agut, M.R. Hamblin, et al. Cationic porphycenes as potential photosensitizers for antimicrobial photodynamic therapy, J. Med. Chem. 53 (2010) 7796-7803.

[26] N. Rubio, F. Prat, N. Bou, J.I. Borrell, J. Teixido, A. Villanueva, et al. A comparison between the photophysical and photosensitising properties of tetraphenyl porphycenes and porphyrins, New J. Chem. 29 (2005) 378-384.

[27] T. Mosmann. Rapid Colorimetric Assay for Cellular Growth and Survival - Application to Proliferation and Cyto-Toxicity Assays, J. Immunol. Methods 65 (1983) 55-63.

[28] N.L. Oleinick, R.L. Morris, I. Belichenko. The role of apoptosis in response to photodynamic therapy: what, where, why, and how, Photochem. Photobiol. Sci. 1 (2002) 1-21.

[29] K. Plaetzer, T. Kiesslich, C.B. Oberdanner, B. Krammer. Apoptosis following photodynamic tumor therapy: Induction, mechanisms and detection, Curr. Pharm. Des. 11 (2005) 1151-1165.

[30] R. Hilf. Mitochondria are targets of photodynamic therapy, J. Bioenerg. Biomembr. 39 (2007) 85-89.

[31] D. Sanchez-Garcia, J.I. Borrell, S. Nonell. One-Pot Synthesis of Substituted 2,2 '-Bipyrroles. A Straightforward Route to Aryl Porphycenes, Org. Lett. 11 (2009) 77-79.

[32] R. Bonnett. Porphyrins and cancer treatment, 89301924.0 (1989).

3.6. ANNEX

Synthesis. Temocene was synthesized using a procedure based in the four-step synthesis of porphycenes recently developed by our group [31] (Fig. A1) and it was performed by Dr. Sánchez-García. Thus the isopropoxy ethers of porphycene were deprotected to the corresponding hydroxy derivative by addition of anhydrous aluminum trichloride to a dichloromethane solution of isopropoxy compound. In order to compare temocene and its chlorin analogue, temoporfin was synthesized using a published procedure [32].

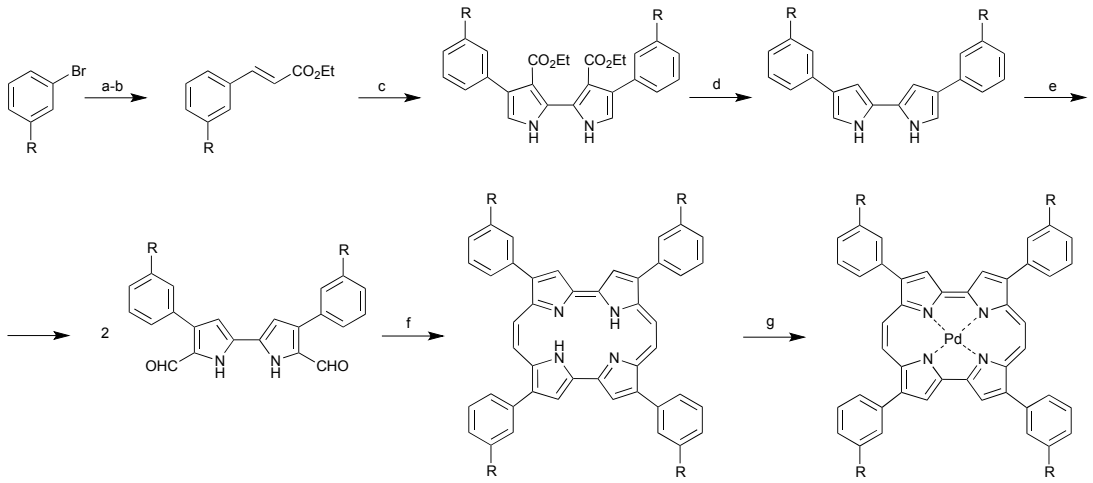

Figure A1. Synthetic pathway used for the synthesis of porphyecenes.

Purity of *m*-THPPo. Liquid chromatography was used to assess the purity of *m*-THPPo. As shown in Fig. A2, a majority peak can be observed at 5.4 min, with a relative integral intensity higher than 97%. The minority peaks observed at 10.0 and 14.3 min have a porphycene-like UV-Vis spectrum and they can be attributed to porphycene aggregates.

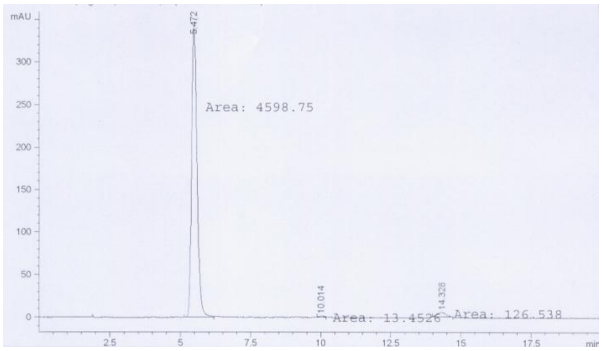

Figure A2. Liquid chromatography of *m*-THPPo detected at 375 nm.

UV-Vis spectra were recorded every 1 s and found to be identical throughout the peak (Fig. A3).

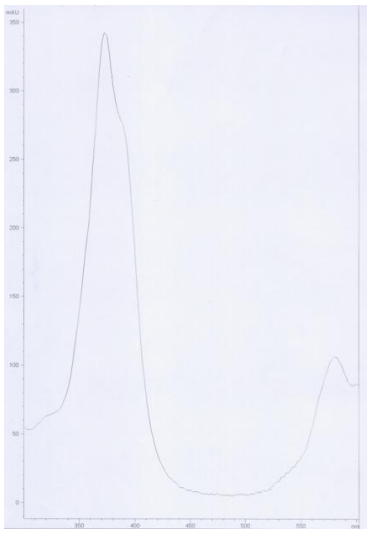

Figure A3. Absorption spectrum of *m*-THPPo peak at 4.3 min obtained by liquid chromatography and diode array detection.

Chapter 4

Liposomes as vehicles for delivery of photosensitizing agents

Developing the ideal formulation

The use of drug delivery systems for photosensitizing drugs has received strong interest within the field of photodynamic therapy (PDT). Liposomes, with their high loading capacity and their flexibility to accommodate different photosensitizers, came into focus as valuable carriers for PDT. This chapter describes the development of two liposomal formulations containing porphycene-based photosensitizers.

4.1. INTRODUCTION

As we have seen in previous chapters, new photosensitizers (PSs) are continuously being developed to enhance their safety and therapeutic efficiency. Most of these PSs are hydrophobic and easily aggregate in aqueous solutions, but the monomeric state is required to maintain their photophysical and biological properties for efficient PDT outcome [1]. Therefore, various pharmaceutical carriers have been developed for the administration of photosensitizers, including oil-based emulsions, polymeric nanoparticles or liposomes.

Liposomes are uni- or multilamellar phospholipid nano-vesicles that allow the incorporation of a great variety of drugs in their matrix because of their particular nature. The lipid bilayer can incorporate highly hydrophobic PSs and prevent their aggregation. On the other hand, the aqueous core is capable of encapsulating water-soluble molecules. Liposomes not only protect PSs from the aqueous environment and metabolic processes, but also provide a large drug payload per particle and improve pharmacokinetics, thus enhancing safety and efficacy of PDT. Moreover, liposomes can prolong the action of drug by slow release of the PS and can modify the internalization and localization once the PS-loaded liposomes reach the targeted cells [2].

Their components (basically natural or synthetic phospholipids) are materials also existing in the body, and therefore provide high biocompatibility and biodegradability [3-5]. The choice of phospholipids and preparation methods are crucial for defining the physical and chemical properties of liposomes, such as size, surface charge density and membrane packing constrains [6]. The lipids normally used are the egg or soybean natural extracts, phosphatidylcholine, phosphatidylethalonamine, phosphatidylserine, phosphatidic acid or phosphatidylglycerol with saturated or unsaturated chains. Cholesterol is often included to stabilize the bilayer [7].

Various preparation methods are available for formulate liposomes of different size and lamellarity. Ethanol injection is probably one of the easiest methods available. It involves the injection of a small volume of ethanolic solution of lipids into a large volume of water. The force of the injection ensures homogeneous mixing of lipids, as does the immediate dilution of the ethanol in the large excess of water. Resulting suspension is then dialyzed in order to remove any trace of remaining ethanol. This procedure generates mainly small unilamellar vesicles with diameters around 25-50 nm [8]. Membrane extrusion is a common method for the preparation of unilamellar

liposomes entrapping hydrophilic drugs. Lipid mixture containing the PS was evaporated to form a dry lipid film, which is hydrated with the desired buffer to form multilamellar vesicles. The suspension is prefiltered through filters with pores ~1 μm followed by several extrusions through filters with a pore size of 0.4 and 0.2 μm. The extrusion method yields the best vesicles with respect to the homogeneity of size distribution and to control the size of vesicles [6]. The method of emulsification also starts from the formation of a dry lipid film that contains the photosensitizer. Hydration is followed by size reduction passing through a high-pressure homogeneizer preheated above the transition temperature of the lipids for several cycles at high pressure (~200 kPa). The advantages of this method are its simplicity for scaleup, large capacity and short preparation times [6]. Sonication method places the multilamellar vesicles suspension in a bath sonicator. Normally a 5-10 min sonication procedure (above the transition temperature of the lipids) is sufficient to prepare small vesicles with a diameter < 100 nm.

Regardless of the preparation method, liposomes are generally classified in three main groups (Fig. 4.1).

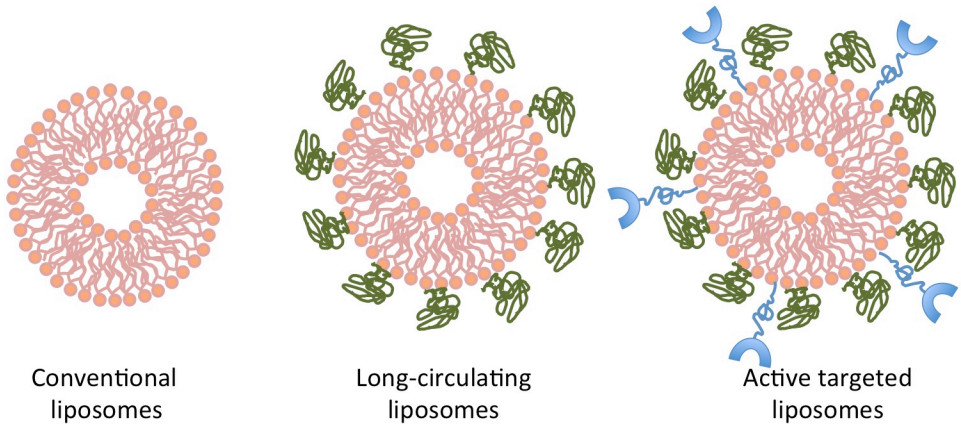

Figure 4.1. Schematic structures of the different types of liposomes.

Conventional liposomes can be defined as liposomes that are typically composed of only phospholipids (neutral and/or negatively charged) and/or cholesterol. They can vary widely in their physicochemical properties such as size, lipid composition, surface charge and fluidity of the bilayer. Although manipulation of these properties can modify, to a certain extent, the *in vivo* behavior of conventional liposomes, conventional

liposomes are characterized by a relatively short blood circulation time [2]. Two different phenomena impair the circulation time of conventional liposomes: the lipid exchange between liposomes and lipoproteins that leads to an irreversible disintegration of the liposomes; and the easy opsonization by plasma proteins leading to the uptake by macrophages of the reticuloendothelial system (RES) [4]. In spite of this fact, conventional liposomes are widely used for *in vitro* conditions. The presence of glycolipids or protective polymers such as polyethylene glycol (PEG) grafted to the liposomal surface increase the circulation half-time to values of up to 12 h [9]. Long-circulating liposomes are also referred as "sterically stabilized" or Stealth® liposomes. With prolonged circulation time, a greater concentration of liposomes can passively accumulate in the tumor by the enhanced permeability and retention (EPR) effect, which increases the amount of PSs available for internalization in tumor cells for improved PDT efficacy. But this passive targeting via the EPR effect may not be sufficient for increasing the amount of PSs internalized into targeted tumor cells. Therefore, active tumor targeting has been explored through liposome surface modification. Cancer cells can be differentiated from surrounding normal cells by various biomarkers, such as overexpressed receptors and enzymes on tumor cells specifically used for their rapid proliferation [10]. Targeting ligands, including antibodies, aptamers, peptides, or small molecules (e.g. folate), grafted to the liposome surface, have been demonstrated to actively target liposomes to diseased tissues [3,4,11]. An extended view of how folate-targeted liposomes could enhance PDT selectivity is described in chapter 5.

We reported in this work the development and optimization of a liposomal formulation for two porphycene-based photosensitizers: Palladium(II)-tetraphenylporphycene (PdTPPo) and *m-(*tetrahydroxyphenyl)porphycene (*m*-THPPo). We have put every effort into obtain long-term stable formulations which incorporate the PS in a monomeric state.

4.2. EXPERIMENTAL SECTION

Materials. Palladium(II)-tetraphenylporphycene (PdTPPo) was synthesized as described previously [12,13]. The synthesis and photophysical characterization of *m-(*tetrahydroxyphenyl) porphycene (temocene, *m*-THPPo) is described in detail in chapter 3. Dimyristoyl-, dipalmitoyl- and distearoylphosphatidylcholine (DMPC, DPPC, DSPC); 1-palmitoyl-2-oleoylphosphatidylcholine (POPC); dimyristoyl-, dipalmitoyl- and distearoylphosphatidylglycerol (sodium salts, DMPG, DPPG, DSPG); 1,2-dioleoylphosphatidylserine (sodium salt, OOPS); 1,2-distearoylphosphatidylethanolamine-N-[methoxy(polyethylene glycol)-3000] (m-PEG_{3000}-DSPE), egg extract phosphatidylcholine (egg-PC) and soy extract phosphatidylcholine (soy-PC) were purchased from Avanti Polar Lipids (Birmingham, AL). Thiobarbituric acid (≥ 98%), trichloroacetic acid (≥ 99%) and malondialdehyde tetrabutylammonium salt (≥ 96%) were purchased from Sigma-Aldrich Chemical Co. (St. Louis, MO). All other chemicals were commercially available reagents of at least analytical grade. Milli-Q water (Millipore Bedford, Massachusetts system, resistivity of 18 MW cm) was used.

Lipid peroxidation measured by TBARS. 500 μL liposome suspension (2 mg/mL) were mixed with 2 mL thiobarbituric reactive species (TBARS) kit (0.375% thiobarbituric acid, 15% trichloroacetic acid, 0.25 M HCl) and were boiled in water for 15 min. The reaction was stopped with ice and centrifuge at 4000 rpm for 10 min. The extent of lipid peroxidation was assessed by comparison between the absorption of this supernatant at 532 nm to that of standard solutions of malondialdehyde (MDA) under the same conditions.

4.3. RESULTS AND DISCUSSION

4.3.1. Palladium porphycene formulation: overcoming the problems

Liposomes containing PdTPPo were prepared by microemulsification. Soy extract phosphatidylcholine (soy-PC) was chosen for these formulations. Its high unsaturation (up to 80% of the lipid components are unsaturated) makes easier the incorporation of molecules with high volume like PdTPPo. Different photosensitizer/lipid molar ratios have been tested ranging from 1:100 to 1:1000. Their characteristics are displayed in Fig. 4.2.

A

Formulation	*L(%)*[a]	*PS(%)*[b]
1:100	84 ± 2	40 ± 2
1:300	76 ± 2	40 ± 2
1:600	85 ± 2	97 ± 2
1:1000	97 ± 2	98 ± 2

[a] L: Lipid content
[b] PS: Photosensitizer content
Data mean ± SD of at least three different measures

B

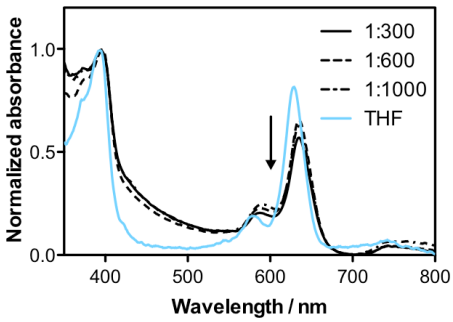

Figure 4.2. Characteristics of PdTPPo/soy-PC formulations. A) Table of characteristics of the different formulations as measured by PS and lipid content. B) Aggregation state of PdTPPo as measured by the changes on absorption spectra of PdTPPo. Spectrum of PdTPPo in THF is given for comparison.

The photosensitizer/lipid molar ratio had great influence on the loading capacity of the vesicles. With an increased number of molecules per liposome (lower molar ratio) the percentage of encapsulated PS decreased dramatically. In contrast, using a molar ratio of 1:600 or 1:1000 we were able to encapsulate ca. 100% of the molecules present at the initial stage of the liposomal formulation. Regarding the aggregation state, we could observe a decrease of the Q band in the absorption spectra of PdTPPo in all cases. However, the spectra did not lose much of the structure, indicating that aggregation occurred but in some extent. The molar ratio PdTPPo/soy-PC of 1:600 was chosen as a good compromise between loading capacity and PS content.

The peroxidation of the lipids in highly unsaturated formulations has been commonly reported [14]. Thus, the stability of formulations was followed by thiobarbituric acid reactive species (TBARS) assay to quantify the formation of end products of lipid peroxidation, specifically malondialdehyde (MDA) (Fig. 4.3).

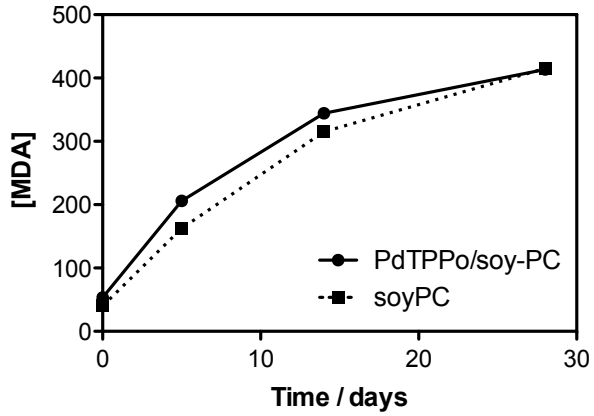

Figure 4.3. Lipid peroxidation of liposomal formulations as function of storage time measured by TBARS assay.

As we can observe in the figure, both PdTPPo/soy-PC and control liposomal formulations were degraded by peroxidation, even when they were storage under nitrogen atmosphere. In order to enhance storage stability, we carried out two different strategies in parallel: change of lipid components and lyophilization of liposomes.

Change of lipid components

Several formulations were tested for the encapsulation of PdTPPo. A summary is given in Table 4.1. In general, the more fluidity of the bilayer, the better encapsulation of the PS in the bilayer. That resulted in better encapsulation yields, better stability after one week and more extent of PS in monomeric state (Fig. 4.4). This fact was also reflected in the size (zeta average) of the liposomes. The formulations with saturated lipids yielded bigger vesicles. These rigid bilayers have to enlarge their radius of curvature in order to accommodate the PdTPPo within. Among all the formulations tested, PdTPPo/POPC/OOPS in 1:450:150 molar ratio can be regarded as a good alternative liposomal composition as it yielded high PS encapsulation and preserved the monomeric state of PdTPPo.

Table 4.1. Physicochemical characteristics of the different formulations as measured by PS and lipid content, particle size and zeta potential

Formulation	*Molar ratio*	*L(%)*[a]	*PS(%)*[b]	*Zave/nm*[c]	ζ_{pot}/*mV*[d]
PdTPPo/DPPC	(1:600)	80 ± 2	60 ± 5[(1)]	250 ± 20	1.2 ± 1
PdTPPo/DMPC/DMPG	(1:540:60)	73 ± 2	60 ± 5[(1)]	180 ± 10	-50 ± 5
PdTPPo/POPC/OOPS	(1:540:60)	76 ± 5	72 ± 5[(1)]	200 ± 10	-32 ± 8
PdTPPo/POPC/OOPS	(1:480:120)	75 ± 5	80 ± 5	177 ± 10	-41 ± 5
PdTPPo/POPC/OOPS	(1:450:150)	87 ± 2	75 ± 5	150 ± 10	-47 ± 5
PdTPPo/Egg-PC	(1:600)	75 ± 2[(2)]	87 ± 5	150 ± 15	-26 ± 5

[a] L: Lipid content
[b] PS: Photosensitizer content
[c] Z average mean
[d] Zeta potential
[(1)] PS=30% after one week
[(2)] Lipid oxidation after one week
Data mean ± SD of at least three different measures

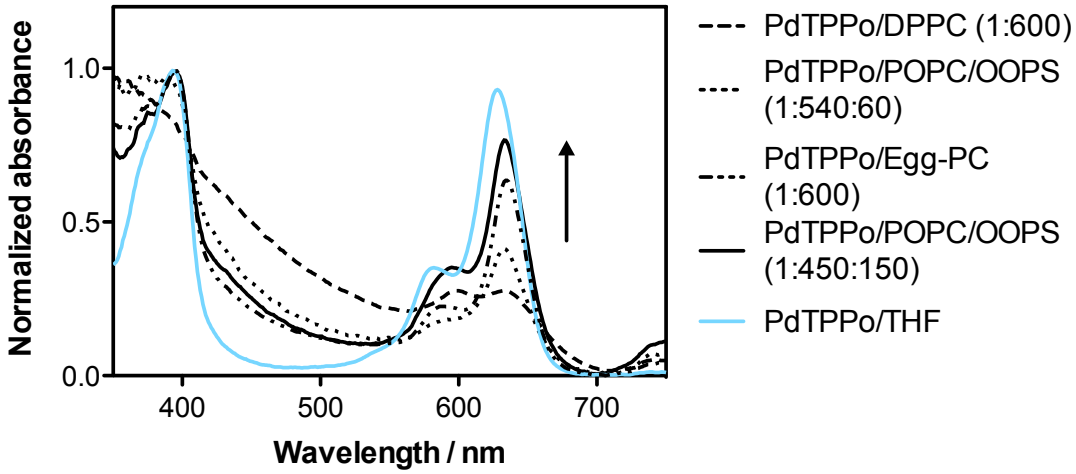

Figure 4.4. Aggregation state of PdTPPo in selected formulations as measured by the changes on absorption spectra of PdTPPo. Spectrum of PdTPPo in THF is given for comparison. Arrow indicates the fluidity of the bilayer in the formulations.

Lyophilization

Lyophilization of the liposomal suspensions is a traditional strategy to ensure the stability of the formulations [15]. There are several parameters affecting the protective effect during liposome lyophilization. In order to choose the optimal formulation and technological parameters for lyophilization process we followed an experimental design based on Taguchi's method $L_9(3^4)$. We defined 4 factors and 3 levels:

- Cryoprotectant: sucrose, trehalose and mannitol.
- % cryoprotectant: 2.5%, 5% and 10%
- Agitation time after hydration: 10, 20 and 30 min
- Storage time: 2, 4 and 6 weeks

Sample: soy-PC liposomes

Following the standard procedure for lyophilization and hydration, we measured the following parameters: size, zeta potential, lipid content and lipid peroxidation (TBARS). Size of the vesicles was highly influenced by the cryoprotectant used as shown in Fig. 4.5A. The other parameters did not show differences independently of the factor used. It is worth noting that the peroxidation was completely avoided with the lyophilization (Fig. 4.5B)

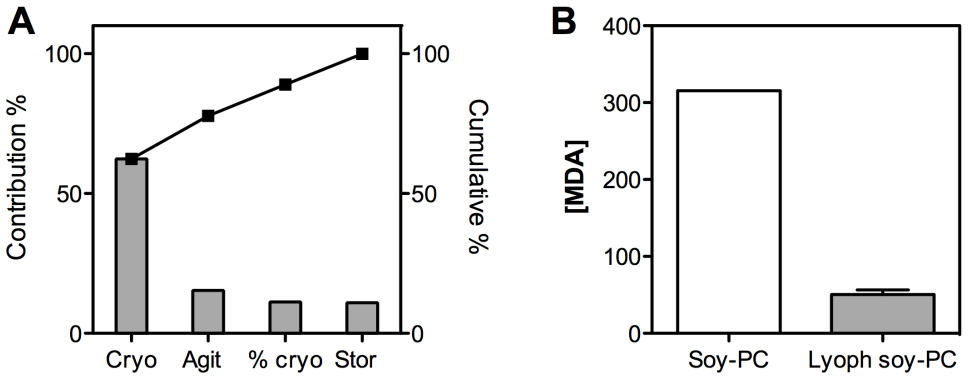

Figure 4.5. A) Pareto analysis of the contribution of each factor to the size of liposomes. B) Lipid peroxidation of liposomal formulations after 2 weeks storage in the fridge or lyophilized.

We considered the following condition as optimal for soy-PC liposome lyophilization: 5% trehalose, 20 min agitation, storage stability > 6 weeks.

Having guaranteed the stability of the formulations, we assessed the dark cytotoxicity and photodynamic action of PdTPPo encapsulated in soy-PC liposomes (Fig. 4.6). Lyophilized formulations were rehydrated just before the experiments. HeLa cells were incubated for 18 h with different concentrations of PdTPPo encapsulated in soy-PC liposomes. Control liposomes without PS were also tested. Afterwards, cells were exposed to 3.5 J/cm^2 red light using a LED source. Cell survival was assessed by MTT assay 24 h after treatment.

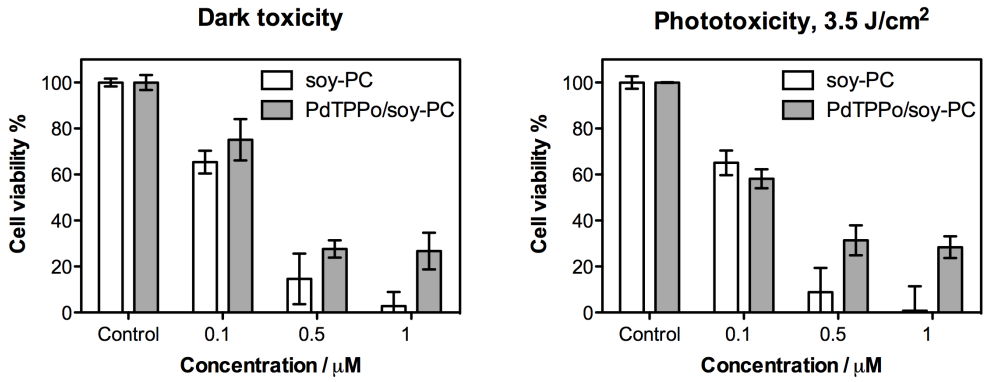

Figure 4.6. Dark and photodynamic induced toxicity of soy-PC liposomes with or without PdTPPo. Mean ± SD from at least three different experiments are shown.

The toxicity induced by the carrier itself was even higher than the PdTPPo containing liposomes. No effect was observed after delivering 3.5 J/cm^2. The drug/lipid molar ratio of these formulations was increased up to 1:600 for an efficient encapsulation of PdTPPo, and therefore, the high concentration of lipids added to the incubation media caused an inherent cytotoxicity. After these results, the formulation was discarded.

4.3.2. Development of temocene liposomal formulation

Temocene is the porphycene analogue to temoporfin (Foscan®). It has been developed a liposomal formulation for this potent PS (Foslip®) in order to avoid problems of drug precipitation after injection [16-18]. Based on these previous works and because temocene is a structural isomer of temoporfin, we first attempted the liposomal formulation using Biolitec's formulation Foslip® (18 mg/mL DPPC, 2 mg/mL DPPG and 1.5 mg/mL *m*-THPC) as reference formulation [19]. Thus, we tested two preparations, *m*-THPPo/DSPC/DSPG (1:10:1.1) and *m*-THPPo/DPPC/DPPG (1:11:1.2), using extrusion or microemulsification methods. Results are summarized in Table 4.2.

Table 4.2. Physicochemical characteristics of the different formulations as measured by PS and particle size.

Formulation	*Method*	*PS (%)*[a]	*Zave/nm*[b]	*Notes*
m-THPPo/DSPC/DSPG (1:10:1.1)	Extrusion	4 ± 5	142 ± 31	PS retained in the filters.
	Microemulsiflication	n.d.	637 ± 52	Very thick suspension
m-THPPo/DPPC/DPPG (1:11:1.2)	Extrusion	18 ± 5	911 ± 270	PS retained in the filters.
	Microemulsification	25 ± 5	1091 ± 400	

[a] PS: Photosensitizer content
[b] Zeta average mean
n.d. Not determined

In this first iteration, extrusion was discarded for controlling the size of the vesicles after hydration. Temocene, because of its high hydrophobicity, was completely retained in the polycarbonate filters of the extruder. Furthermore, the formulation *m*-THPPo/DSPC/DSPG was also discarded. Its high phase transition temperature (above 45ºC [16]) made the suspension as a solid gel, not suitable for injectable formulations.

In a second approach, lipid mixtures of different chain length were tested. Phospholipid chains of different length cause discontinuities in the lipid membrane where the photosensitizer can accommodate. As we can see in Table 4.3, PS encapsulation yields have improved considerably but they were still too low. Moreover, the resulting liposomes were too large with high polydispersity. This indicated that the radius of curvature is very constrained and therefore the bilayer could not accommodate many PS molecules resulting in a low encapsulation yield and large vesicles.

Table 4.3. Physicochemical characteristics of the different formulations as measured by PS and particle size.

Formulation	*PS (%)*[a]	*Zave/nm*[b]	*Notes*
m-THPPo/DSPC/DMPG (1:10:1.3)	30 ± 10	155 ± 30	PS aggregated.
m-THPPo/DPPC/DMPG (1:11:1.3)	52 ± 13	186 ± 50	PS aggregated.
m-THPPo/DPPC/DPPG (1:11:1.2)	47 ± 5	246 ± 100	Too polydispersed.
m-THPPo/DMPC/DMPG (1:12:1.3)	58 ± 10	224 ± 45	Too polydispersed.
m-THPPo/POPC/OOPS (1:9:1)	34 ± 10	363 ± 45	Too polydispersed.

[a] PS: Photosensitizer content
[b] Zeta average mean

Increasing the drug/lipid relation to 1:25 we obtained better encapsulation yields but the size of liposomes was still too large and too polydispersed (Table 4.4).

Table 4.4. Physicochemical characteristics of the different formulations (PS/lipid molar ratio 1:25) as measured by PS and particle size.

Formulation	*PS (%)*[a]	*Zave/nm*[b]	*Notes*
m-THPPo/DPPC/DPPG (1:22.5:2.5)	72 ± 8	212 ± 80	Too polydispersed.
m-THPPo/DPPC/DMPG (1:22.5:2.5)	65 ± 10	120 ± 50	
m-THPPo/DMPC/DMPG (1:22.5:2.5)	66 ± 15	224 ± 80	Too polydispersed.
m-THPPo/POPC/OOPS (1:22.5:2.5)	88 ± 5	470 ± 90	Too polydispersed.

[a] PS: Photosensitizer content
[b] Zeta average mean

The best results were obtained with DPPC/DMPG formulation, although the temocene content is still low. The drug/lipid molar ratio was then increased to 1:75 and 1:100 using this formulation (Table 4.5). Both liposomal suspensions showed good encapsulation yields with a vesicle size close to 120 nm. We chose *m*-THPPo/DPPC/DMPG (1:67.5:7.5) as the optimal formulation for the encapsulation of temocene.

Table 4.5. Physicochemical characteristics of *m*-THPPo/DPPC/DMPG formulations as measured by PS and particle size.

Formulation	***PS (%)[a]***	***Zave/nm[b]***
m-THPPo/DPPC/DMPG (1:67.5:7.5)	89 ± 10	117 ± 40
m-THPPo/DPPC/DMPG (1:90:10)	95 ± 10	123 ± 34

[a] PS: Photosensitizer content
[b] Zeta average mean

The local concentration of the solubilized porphycene in the liposome bilayer can be estimated by means of the total number of lipid molecules per liposome (N_{lip}). N_{lip} can be calculated using the following equation (Eq. 4.1) [20]:

$$N_{lip} = \frac{4\pi\left(\frac{D_H}{2}\right)^2 + 4\pi\left(\frac{D_H - h}{2}\right)^2}{a} \qquad (4.1)$$

where D_H is the hydrodynamic diameter, h is the thickness of the bilayer (3.7 nm for DPPC vesicles [21]) and a is the cross-sectional area of the polar head of lipids (0.71 nm^2 for phosphatidylcholine [22]). Considering our liposomes are composed only by DPPC lipids, the number of lipid molecules per liposome is N_{lip} = 119 817 molecules. Since the molar ratio PS/lipid is 1:75, the number of photosensitizer molecules in a liposome is N_{PS} = 1597 molecules (2.6 x 10^{-21} mol). The volume of a liposome is calculated as follows (Eq. 4.2):

$$V = 4/3\pi(\tfrac{D_H}{2})^3 - 4/3\pi(\tfrac{D_H - h}{2})^3 \qquad (4.2)$$

The volume of a liposome is therefore 1.6 x 10^{-19} L. Thus, the local concentration of temocene in a liposome of 120 nm diameter is 0.016 M. This high local concentration of temocene inside the liposome can influence the photophysical properties of the PS.

As we observed in Fig. 4.7 temocene in liposomes presented a structured absorption spectra without presence of any additional bands typical of aggregates. This result evidenced that although the high local concentration, the PS is still in a monomeric state.

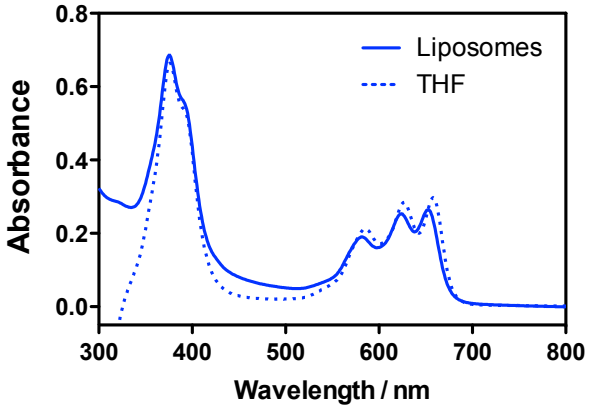

Figure 4.7. Absorption spectra of temocene in DPPC/DMPG liposomes and in THF.

The absorption spectrum measured of liposomes included two contributions: absorption of encapsulated temocene and scattering of the vesicles, the latter more evident at lower wavelengths. The determination of fluorescence quantum yield (Φ_F) was therefore influenced by this fact. It was calculated from the comparison of the area under the emission curve of optically-matched solutions of the sample to that of a reference, in this case, cresyl violet (CV) (Fig. 4.8).

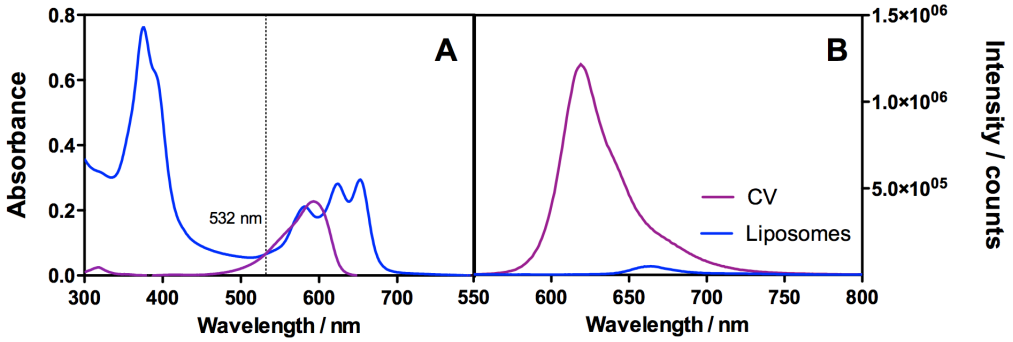

Figure 4.8. Absorption (A) and emission (B) spectra of cresyl violet in MeOH (violet) and temocene encapsulated in liposomes (blue).

Considering that there would be less molecules of photosensitizer than that we were adjusting because of the scattering contribution, we expressed the fluorescence quantum yield as $\Phi_F \geq 0.02 \pm 0.003$.

The same holds true for the singlet oxygen quantum yield (Φ_Δ) (Fig. 4.9) and therefore it was expressed as $\Phi_\Delta \geq 0.082 \pm 0.02$.

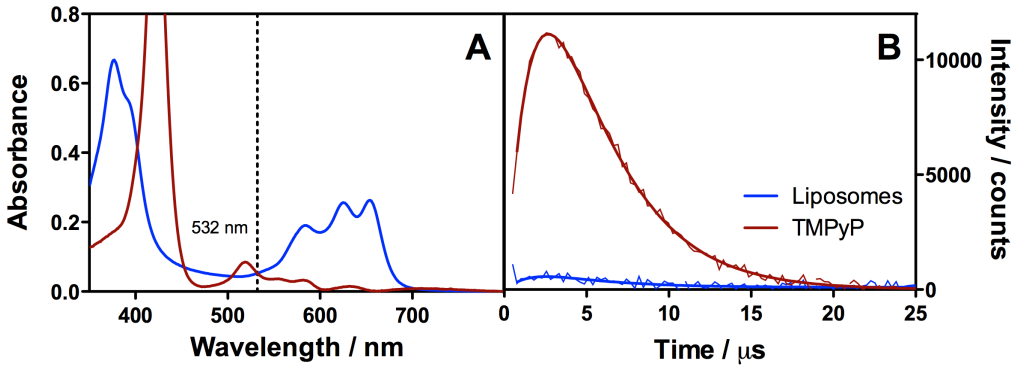

Figure 4.9. Absorption (A) and singlet oxygen phosphorescence (B) spectra of TMPyP in water (red) and temocene encapsulated in liposomes (blue).

The singlet lifetime of temocene encapsulated in liposomes decayed with a lifetime of $\tau_S = 1.6 \pm 0.2$ ns (Fig. 4.10), substantially lower than that of temocene in THF ($\tau_S = 2.3 \pm 0.2$ ns).

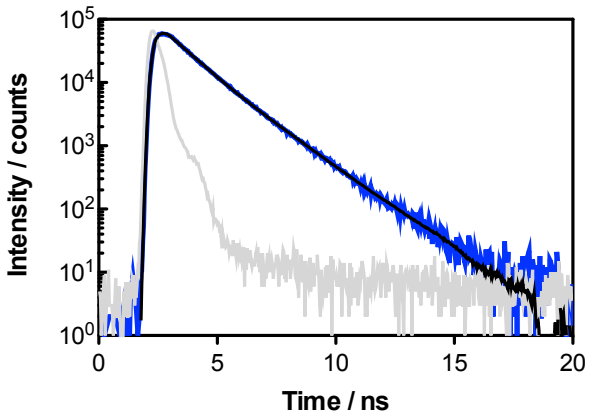

Figure 4.10. Fluorescence decay of temocene encapsulated in liposomes (λ_{exc} = 375 nm, λ_{em} = 660 nm)

Although the PS was apparently in a monomeric state regarding its absorption spectrum, the fluorescence and singlet oxygen quantum yields and the singlet lifetime of temocene inside the liposomes indicated that liposomes affected in some extent the photophysical characteristics of the photosensitizer. This effect could be due to the high local concentration of the temocene inside the liposomal bilayer (16 mM) and therefore the formation of dimers, trimmers and high order aggregates can occur. A

similar effect was observed for liposomal encapsulated chlorins [23]. The high local concentration of the PS induced remarkable changes in the photophysical properties. However, after being incorporated to human skin fibroblasts, the PSs existed as monomers inside the cells showing the same photophysical properties as in organic solution. We can expect the same result for the temocene formulation.

Lyophilization

An ideal formulation should be endowed with long-term stability and easy manipulation. Many methods are available for liposome stabilization such as freezing or spray-drying, though lyophilization is the main approach used to extent the self-life of liposomes [15]. Using the conditions optimized for soy-PC liposomes (5% trehalose as cryoprotectant and 20 min agitation during hydration), we studied the effect of lyophilization process on the physicochemical properties of the temocene liposomal formulation (Table 4.6).

Table 4.6. Effect of lyophilization on the physicochemical characteristics of temocene liposomal formulation.

Formulation	***PS (%)*** [a]	***L (%)*** [b]	***Zave/nm*** [c]	***ζpot/mV*** [d]
Liposomes	95 ± 2	90 ± 5	117 ± 40	-73 ± 5
Liposomes after lyophilization/rehydration	90 ± 5	82 ± 5	190 ± 40	-65 ± 8

[a] PS: Photosensitizer content
[b] L: Lipid content
[c] Zeta average mean
[d] Zeta potential

As expected, the size of liposomes was increased due to the fusion/aggregation of vesicles although it was maintained within the optimal size range for cellular internalization. Neither the PS content nor the aggregation state was influenced by lyophilization. This process ensured the stability of liposomal formulations during several months of storage.

4.4. CONCLUSIONS

In this work, we have faced up to the development of different liposomal formulations for the delivery of two porphycene-based photosensitizers: PdTPPo and *m*-THPPo.

The effect of palladium coordination was not only reflected in the photophysical properties of the porphycene, but also in its liposomal encapsulation. The insertion of the metal ion in the macrocycle cavity distorted the geometry of the macrocycle core and therefore its planarity [24]. This distortion hampered its packaging within the lipid bilayer, decreasing the number of PS molecules per liposome. We found 1:600 a drug/lipid molar ratio that allowed high PdTPPo encapsulation yields with minimal aggregation. We used highly unsaturated lipids with high fluidity (phosphatidylcholine soy extract) to facilitate the incorporation of the photosensitizer. However, these unsaturations led to the peroxidation of the lipids. To enhance the stability of the formulations we proposed two strategies: change the lipid components to lower unsaturated chains that avoid peroxidation (PdTPPo/POPC/OOPS, 1:450:150 molar ratio) or lyophilize the soy-PC liposomal formulation. We have optimized the parameters for an optimal lyophilization of the liposomal formulations. However, the reconstituted liposomal suspension was not suitable for cellular experiments since it was cytotoxic by itself.

We also developed the liposomal formulation for temocene. We found that *m*-THPPo/DPPC/DMPG (1:67.5:7.5 molar ratio) yielded a high encapsulation rate with liposome sizes of ca. 120 nm. The local concentration of temocene inside the liposomal bilayer was 16 mM. This high concentration could lead to the formation of aggregates affecting the photophysical properties of temocene in some extent. In spite of this fact, we assumed that DPPC/DMPG liposomes are a good drug delivery system for temocene photosensitizer that fulfills the requirements of an ideal carrier for PDT: avoid aggregation of the PS in aqueous environments providing a high drug payload. The influence of liposomes in internalization, subcellular localization and *in vivo* pharmacokinetics will be discussed in chapter 6.

4.5. REFERENCES

[1] Y.N. Konan, R. Gurny, E. Allemann. State of the art in the delivery of photosensitizers for photodynamic therapy, J. Photochem. Photobiol. B: Biol. 66 (2002) 89-106.

[2] G. Storm, D. Crommelin. Liposomes: quo vadis? Pharm. Sci. Technol. Today. 1 (1998) 19-31.

[3] C.S. Jin, G. Zheng. Liposomal nanostructures for photosensitizer delivery, Lasers Surg. Med. 43 (2011) 734-748.

[4] A.S.L. Derycke, P.A.M. de Witte. Liposomes for photodynamic therapy, Adv. Drug Deliv. Rev. 56 (2004) 17-30.

[5] P. Machy, L. Leserman, Liposomes in cell biology and pharmacology, Eurotext, Londres, 1987.

[6] S. Chatterjee, D.K. Banerjee. Preparation, isolation, and characterization of liposomes containing natural and synthetic lipids, Methods Mol.Biol. 199 (2002) 3-16.

[7] S. Vemuri, C.T. Rhodes. Preparation and characterization of liposomes as therapeutic delivery systems: a review, Pharm. Acta Helv. 70 (1995) 95-111.

[8] C.R. Dass. Drug delivery in cancer using liposomes, Methods Mol. Biol. 437 (2008) 177-182.

[9] D.D. Lasic, F.J. Martin, A. Gabizon, S.K. Huang, D. Papahadjopoulos. Sterically stabilized liposomes: a hypothesis on the molecular origin of the extended circulation times, Biochim. Biophys. Acta. 1070 (1991) 187-192.

[10] W.M. Sharman, J.E. van Lier, C.M. Allen. Targeted photodynamic therapy via receptor mediated delivery systems, Adv. Drug Deliv. Rev. 56 (2004) 53-76.

[11] P. Sapra, T.M. Allen. Ligand-targeted liposomal anticancer drugs, Prog. Lipid Res. 42 (2003) 439-462.

[12] M. Cañete, A. Ortiz, A. Juarranz, A. Villanueva, S. Nonell, J.I. Borrell, et al. Photosensitizing properties of palladium-tetraphenylporphycene on cultured tumour cells, Anticancer Drug Des. 15 (2000) 143-150.

[13] N. Rubio, F. Prat, N. Bou, J.I. Borrell, J. Teixido, A. Villanueva, et al. A comparison between the photophysical and photosensitising properties of tetraphenyl porphycenes and porphyrins, New J. Chem. 29 (2005) 378-384.

[14] R. Pamplona, M. Portero-Otin, J.R. Requena, S.R. Thorpe, A. Herrero, G. Barja. A low degree of fatty acid unsaturation leads to lower lipid peroxidation and lipoxidation-derived protein modification in heart mitochondria of the longevous pigeon than in the short-lived rat, Mech. Ageing Dev. 106 (1999) 283-296.

[15] C. Chen, D. Han, C. Cai, X. Tang. An overview of liposome lyophilization and its future potential, J. Control. Release 142 (2010) 299-311.

[16] J. Kuntsche, I. Freisleben, F. Steiniger, A. Fahr. Temoporfin-loaded liposomes: physicochemical characterization, Eur. J. Pharm. Sci. 40 (2010) 305-315.

[17] D. Kachatkou, S. Sasnouski, V. Zorin, T. Zorina, M.A. D'Hallewin, F. Guillemin, et al. Unusual photoinduced response of mTHPC liposomal formulation (Foslip), Photochem. Photobiol. 85 (2009) 719-724.

[18] H.P. Lassalle, D. Dumas, S. Grafe, M.A. D'Hallewin, F. Guillemin, L. Bezdetnaya. Correlation between in vivo pharmacokinetics, intratumoral distribution and photodynamic efficiency of liposomal mTHPC, J. Control. Release. 134 (2009) 118-124.

[19] V. Albrecht, A. Fahr, D. Scheglmann, S. Gräfe, W. Neuberger. Liposomal formulations of hydrophobic photosensitizer for photodynamic therapy, (2008) US7354599.

[20] D.D. Lasic, Liposomes : from physics to applications, Elsevier, Amsterdam; New York, 1993.

[21] Y. Tahara, Y. Fujiyoshi. A new method to measure bilayer thickness: cryo-electron microscopy of frozen hydrated liposomes and image simulation, Micron. 25 (1994) 141-149.

[22] J.N. Israelachvili, D.J. Mitchell. A model for the packing of lipids in bilayer membranes, Biochim. Biophys. Acta. 389 (1975) 13-19.

[23] F. Postigo, M.L. Sagrista, M.A. De Madariaga, S. Nonell, M. Mora. Photosensitization of skin fibroblasts and HeLa cells by three chlorin derivatives: Role of chemical structure and delivery vehicle, Biochim. Biophys. Acta. 1758 (2006) 583-596.

[24] E. Vogel. Novel porphyrinoid macrocycles and their metal complexes, J. Heterocycl. Chem. 33 (1996) 1461-1487.